UNIVERSITY OF CALIFORNIA, SAN DIEGO

Electrical and thermal percolation in carbon nanotube-polymer composites

A dissertation submitted in partial satisfaction of the

requirements for the degree Doctor of Philosophy

in

Materials Science and Engineering

by

Byung-Wook Kim

Committee in Charge:

Professor Prabhakar Bandaru, Chair
Professor Renkun Chen
Professor Sungho Jin
Professor Ratneshwar Lal
Professor Yu Qiao
Professor Donald Sirbuly

2014

The dissertation of Byung-Wook Kim is approved, and it is acceptable in quality and form for publication on microfilm and electronically:

Chair

University of California, San Diego

2014

DEDICATION

Dedicated to my loving wife and my family

who have always shown unfailing love and support

TABLE OF CONTENTS

LIST OF FIGURES

ACKNOWLEDGEMENTS

During my graduate studies at University of California at San Diego, I have been blessed to meet so many talented people. Firstly, I cannot thank my advisor enough for being my mentor; I would like to express my sincerest gratitude to Professor Prabhakar R. Bandaru for giving me a wonderful opportunity to be part of the greatest journey that I have experienced thus far. Her heartfelt encouragement, guidance, and passion for science always inspire me to joyfully follow my own trail without any hesitation.

I would like to thank my committee members, Prof. Sungho Jin, Prof. Ratneshwar Lal, Prof. Yu Qiao, Prof. Renkun Chen, and Prof. Donald J. Sirbuly for helpful discussions and suggestions on my dissertation. In particular, I am truly grateful to Prof. Sungho Jin for the constructive guidance in research and the provided support in my future career.

I am indebted to all my former and present members of the Bandaru group who are my colleagues: Dr. Sung-Hoon Park for being a dependable friend and for teaching me nanotube/polymer composite synthesis, Dr. Steven Pfeifer for showing me how to measure high resistance materials, Dr. Max Aubain for their participation and the insightful discussion, and Dr. Paothep Pichanusakorn, Dr. Rahul Kapadia, Dr. Hasan Faraby, Anna Alexander, Krishna Vemuri, Rajaram Narayanan, David Moreira, Hidenori Yamada, Thomas Hall, Francisco Mancillas, and Mehmet Canbazoglu for the support they have provided over the many years.

I would like to recognize and thank Charlotte Lauve for the administrative paperwork, invaluable advice, and numerous informative notices.

Lastly, I would like to express my deepest gratitude and love to my wife, Jihyun Lee, and my family: Hyunjung Kim, Junghee Han, Byungsoo Kim for their unfailing love, support, and prayer.

Chapter 2, in part, is a reprint of the material as it appears in the following publication: B.-W. Kim, S. Pfeifer, S.-H. Park, P. R. Bandaru, "Experimental determination of the onset of electrical and thermal conductivity percolation thresholds in carbon nanotube-polymer composites." *Mater Res Soc Symp Proc.* **1312** 2011. doi:10.1557/opl.2011.114. The dissertation author was the primary investigator and author of this paper.

Chapter 3, in full, is a reprint of the material as it appears in the following publication: B.-W. Kim, S.-H. Park, R. S. Kapadia, P. R. Bandaru, "Evidence of percolation related power law behavior in the thermal conductivity of nanotube/polymer composite." *Appl Phys Lett*. **102** 243105 (2013). doi: 10.1063/1.4811497. The dissertation author was the primary investigator and author of this paper.

Chapter 4, in full, is a reprint of the material as it is under preparation for publication: B.-W. Kim, S.-H. Park, P. R. Bandaru, "Anomalous decrease of the specific heat capacity at the electrical and thermal conductivity percolation threshold in nanocomposites." The dissertation author was the primary investigator and author of this paper.

VITA

2007	Bachelor of Science in Physics,
	Hanyang University, Korea
2011	Master of Science in Electrical and Computer Engineering,
	University of California, San Diego
2014	Doctor of Philosophy in Materials Science and Engineering,
	University of California, San Diego

PUBLICATIONS

1. Kim, B.-W., Pfeifer, S. Park, S.-H. & Bandaru, P. R. Experimental determination of the onset of electrical and thermal conductivity percolation thresholds in carbon nanotube-polymer composites. *Mater Res Soc Symp Proc.* **1312** 2011.

2. Kim, B.-W., Park, S.-H., Kapadia, R. S. & Bandaru, P. R. Evidence of percolation related power law behavior in the thermal conductivity of nanotube/polymer composite. *Appl Phys Lett*. **102** 243105 (2013).

3. Kim, B.-W., Park, S.-H. & Bandaru, P. R. Anomalous decrease of the specific heat capacity at the electrical and thermal conductivity percolation threshold in nanocomposites. *submitted*

4. Park, S.-H., Theilmann, P., Kim, B.-W., Yun, D.-J. & Bandaru, P. R. Enhanced electromagnetic interference shielding and dispersion condition through the use of coiled carbon nanotube polymer composites. *under preparation*

ABSTRACT OF THE DISSERTATION

Electrical and thermal percolation in carbon nanotube-polymer composites

by

Byung-Wook Kim

Doctor of Philosophy in Materials Science and Engineering

University of California, San Diego, 2014

Professor Prabhakar R. Bandaru, Chair

Electrical and thermal properties of carbon-nanotube (CNT)/polymer composites were investigated through percolating behavior of conducting fillers in insulating matrix. Synthesis methodology has been found using a blend of solution processing, which was adapted to facilitate uniformly distributed CNTs in polymer matrix and consequently to contribute to percolation. The onset of percolation thresholds depending on aspect ratio of fillers were theoretically estimated by the excluded volume method as well as experimentally examined with a power relation of the both electrical and thermal conductivities. Consistent modeling of the both electrical and thermal conductivity anisotropy, in addition to the incorporation of interfacial resistance between connected

conducting CNT fillers, was used to understand the underlying transport mechanisms and variations.

Furthermore, we report a decrease in the specific heat capacity of the composites at a particular nanotube filler fraction, corresponding to the electrical and thermal conductivity percolation threshold. Extensive calibration and characterization of two different methods were accomplished for the specific heat capacity measurement, and degree of crystallinity through x-ray diffraction implied how degree of disorder would alter depending on arranging nanotubes in the polymer matrix. We explained such change in terms of the entropic configuration determined by number of isolated or connected nanotube fillers.

Our investigations could yield better insight into percolation phenomena, of wide importance in the theory of networks, and the optimal conditions of CNT connectivity and dispersion for various applications.

CHAPTER 1: Experimental challenges of the dissertation

This chapter describes background information about thermal conductivity measurement and discusses the experimental challenges with the corresponding found solution process in each measurement.

1.1 3ω method for thermal conductivity

1.1.1 Background of thermal conductivity measurement

Since heat transfers through three different ways which are radiation, convection, and conduction, it is necessary to reduce/eliminate radiation and convective effect for measuring actual thermal conductivity, and 3ω methodology has been known to be appropriate for this purpose, since D. G. Cahill reported use of the technique to measure thermal conductivity of non-conducting solids in 1987.[1] When generating AC current through a thin and long metal line placed on specimen, electrical resistance of the line heater oscillates in the response of specimen at the second harmonic due to Joule heating. In turn, the third harmonic voltages, product of the first harmonic current and the second harmonic resistance, would be experimentally detected to acquire the temperature oscillation as a function of frequency. An analytical solution of heat transfer equation in a cylindrical coordinate system was obtained to find the corresponding thermal conductivity by equating the measured temperature oscillation to the theoretical one given frequency range.

1.1.2 Metal line fabrication

Although photolithography is standard to fabricate metal lines for the 3ω technique,[1, 2] we develop another method for flexible materials having low melting point. When a photolithography recipe was applied for such materials, for instance Reactive ethylene terpolymer (RET), unavoidable cracks were generated during lift-off or when carrying samples between processes, as well as the materials was deformed due to applied heat during metal deposition without cooling or resting. Thus, a stainless steel shadow mask containing different dimensions of the line pattern was designed to solve

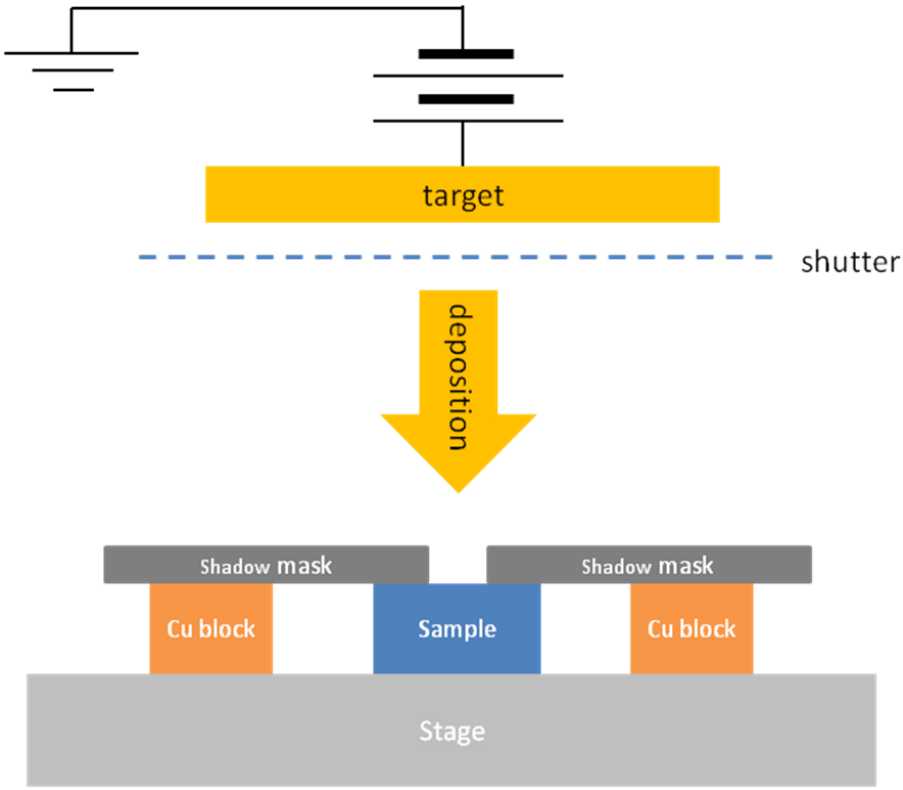

Figure 1. 1. Schematic of DC sputtering: metal deposition through shadow mask with copper block incorporation.

the problem of cracks in metal lines without lift-off process, so that 70 μm wide and 10 mm long lines were found to be optimal based on calibration results with Pyrex, and metal deposition process was developed for either sputtering or electron-beam (e-beam) evaporation: resting/cooling steps were inserted to dissipate excess heat on to the shadow mask for sputtering (Figure 1. 1)/e-beam evaporation (Figure 1. 2).

When loading the polymer or composite materials, copper blocks were placed and attached between the mask and stage as a heat sink, helping to spread heat down to the

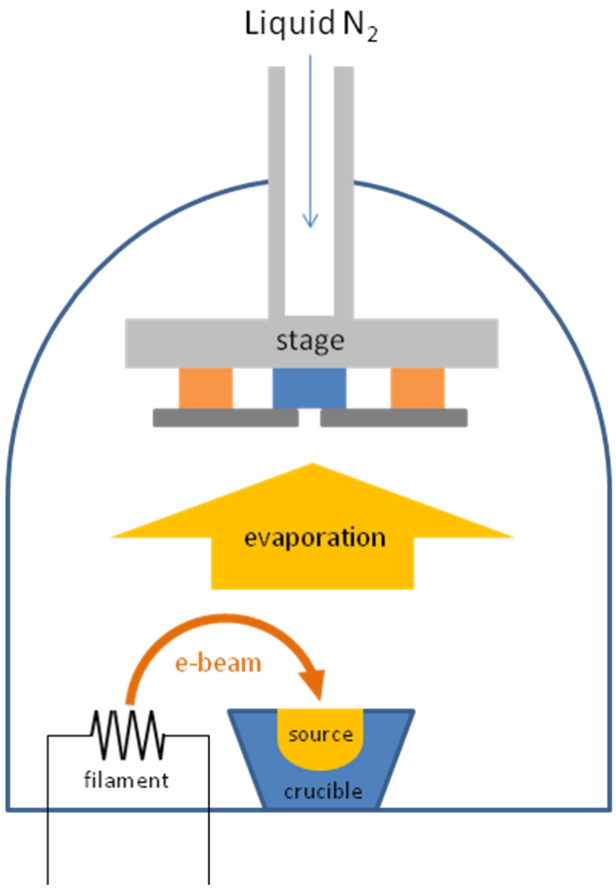

Figure 1. 2. Schematic of e-beam evaporation with liquid N_2 cooling

stage. For metal (Ti and Au) deposition, liquid nitrogen kept cooling down the stage with e-beam evaporation, and the shutters of Ti and Au sputter guns were closed to rest samples for 2 min every 10 seconds deposition with sputtering. Hence, temperature of the materials maintains below melting point in the both metal deposition processes without any deformation, and immaculate metal crack.

1.1.3 Wire bonding

Since the Au metal contacts on the flexible materials are still easy to break with external force and pressure, the contacts were punctured by Au wire bonding (West Bond Wedge Bonder), so after those were initially attached to sliver wires with the electrically conductive epoxy (Epoxy Technology EPO-TEK H20E silver epoxy), the epoxy mixture was solidified at room temperature for 24 hours.

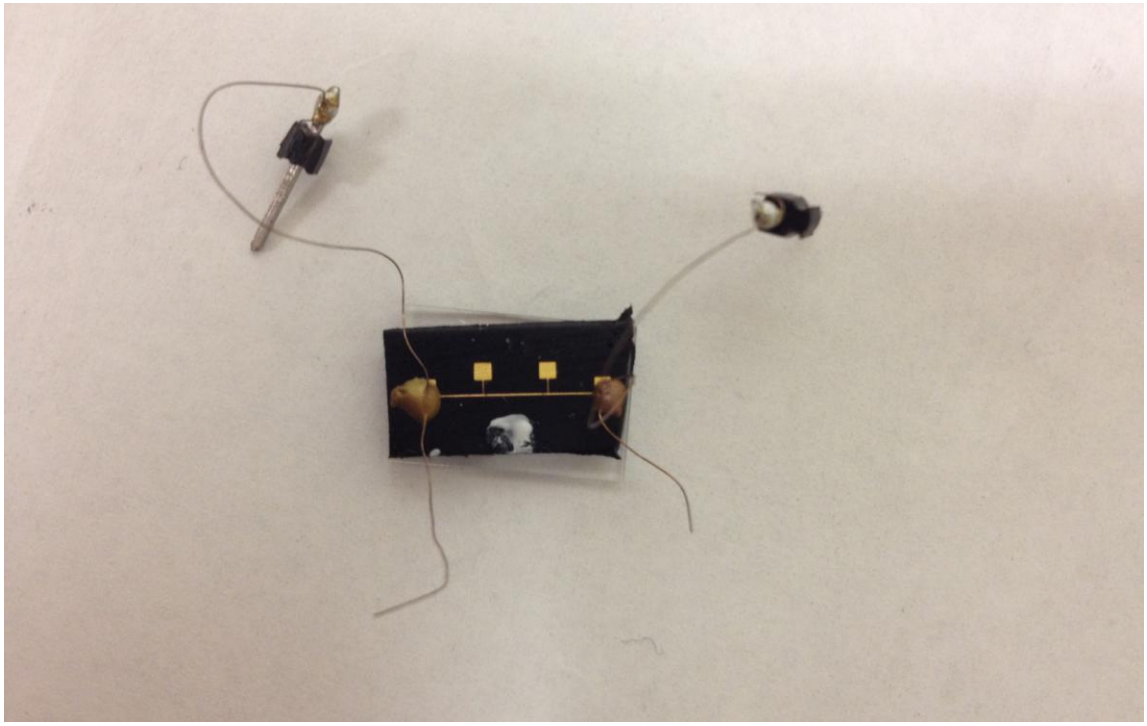

Figure 1. 3. Image of epoxy wire bonding.

1.1.4 Temperature coefficient of resistance

Measuring temperature coefficient of resistance of the line heater was done prior to 3ω method. While a sample mounted on a thermoelectric cooler/heater was cooled/heated by changing applied DC current from -1 mA to +1 mA through Keithley 2400 Source-meter, both the sample temperature and resistance were measured by a K-type thermocouple touching the sample surface and four-point measurement, respectively, after reaching steady-state in 5 min at each temperature. Figure 1. 4 shows the measured resistance of the metal line at different temperature, and the least-square method was used to find the slope, thus the corresponding temperature coefficient of resistance.

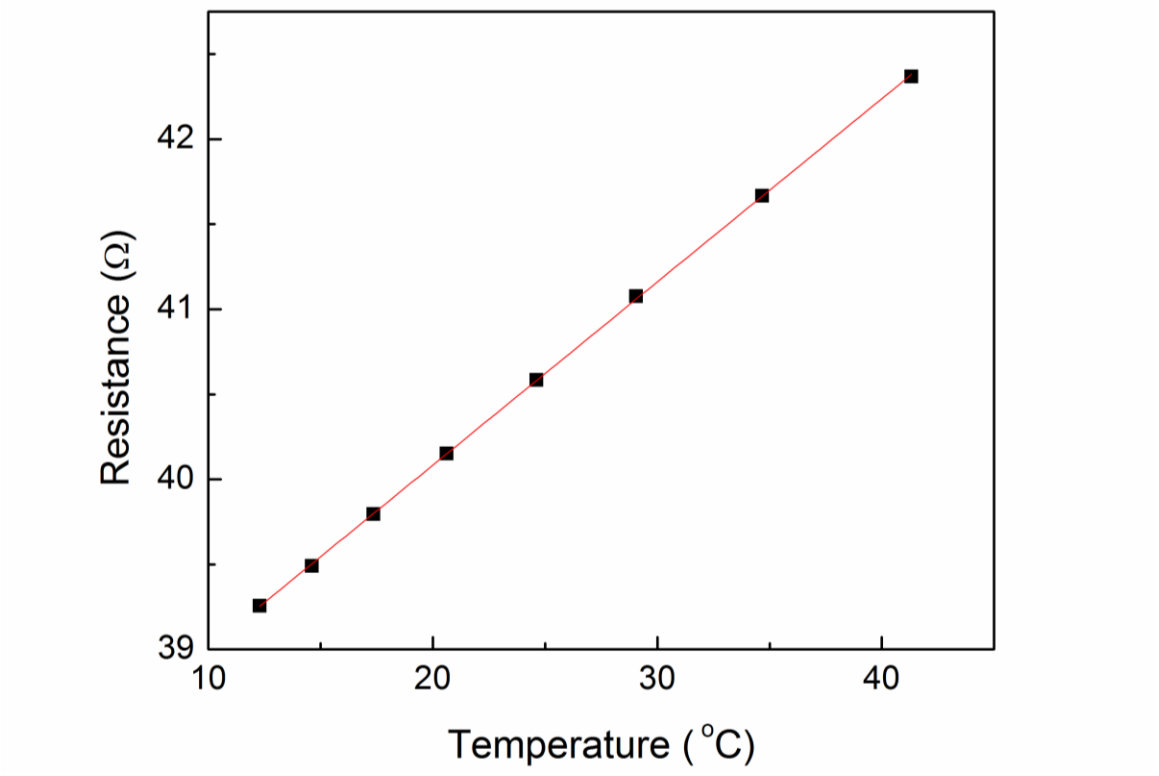

Figure 1. 4. Resistance of Ti/Au metal line on RET around room temperature. Square black dots are measured resistance at different temperature and red solid line is the linear fit by least-square method.

1.1.5 Wheatstone bridge and differential amplifier circuitry with lock-in amplifier

Before acquiring 3ω voltages with a lock-in amplifier, Stanford Research Systems SR830, Wheatstone bridge or differential amplifier circuitry was constructed to attenuate the first harmonic voltage (V_ω), which is the main noise in the 3ω methodology, coming from the function generator. As the noise amplitude is generally 3 orders of magnitude greater than the amplitude of the third harmonic signal, built-in bandwidth filter of the lock-in amplifier was not enough to increase signal-to-noise ratio. Figure 1. 5 shows that 3ω component ($V_{3\omega}$) of across the sample (R_s) was obtained from measuring voltage difference (V_A-V_B) through the lock-in amplifier inputs when the left arm and right arm were balanced by changing resistance (R_1) of the potentiometer.

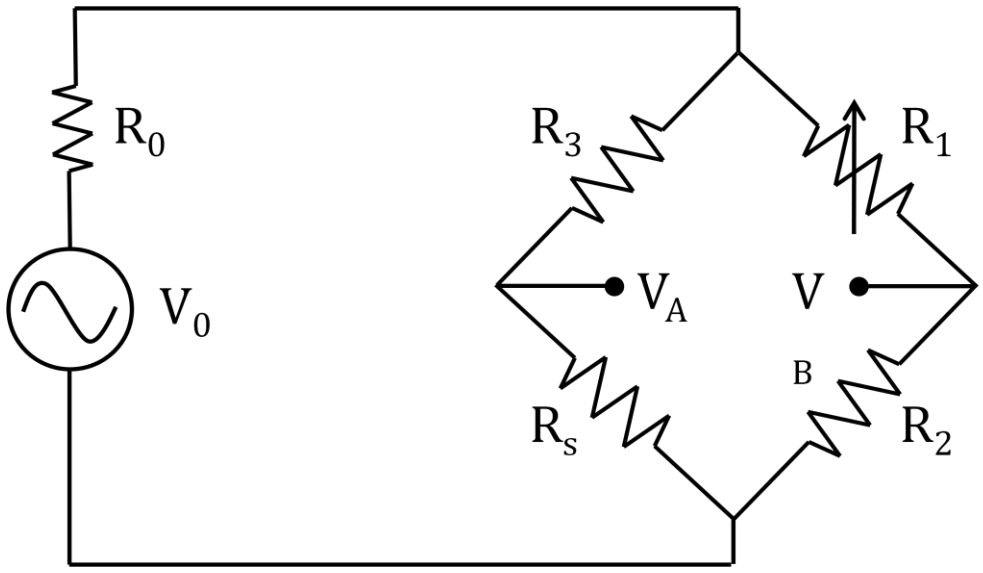

Figure 1. 5. Schematic of the Wheatstone bridge based apparatus for measuring thermal conductivity with the 3ω method. The bridge serves to nullify the larger first harmonic component V_ω.

Instead of an external function generator, due to low harmonic distortion internal AC voltage source V_o of the lock-in amplifier was connected across the Wheatstone bridge (in Figure 1.5). Besides, beneficial functions of SR830 were found to read correct signals with suitable combination. A -24 dB/oct low pass filter, the steepest slope mode, was selected to attenuate the first harmonic noise, appropriate time constant and stabilization time were important to read the third harmonic signals. For example, when reading $V_{3\omega}$ at 1 Hz or below of the function generator, the signal would be stabilized in 3 minutes with 10 seconds of time constant, while 1 second constant and 10 seconds stabilization were used 1k Hz or above.

1.1.6 Automation

The entire measurement system was automated by a computer which is connected with SR830 via General Purpose Interface Bus (GPIB) using a custom LabVIEW virtual instrument. The following is the algorithm of measurement.

1. 2 Scanning electron microscopy (SEM) for polymeric materials

In general, electrically conducting solid materials is suitable to be used in scanning electron microscopy. However, we experimentally prepared polymeric materials in order to see dispersion of conducting fillers within insulating polymeric matrix in this study. It was necessary to bisect such elastic materials without affecting structural modification by external force, such as pressing down with a razor blade or scissors. About 300 micrometer thick polymeric materials were clipped with two tweezers after being frozen enough within liquid N_2 for 2 minutes.

Since reactive ethylene terpolymer (RET) whose conductivity and melting point are low, we were not able to observe its structure because of charging effect, and its surface was deformed as irradiated electron beam caused heat to the materials. Thus, the materials samples were gold-coated using sputtering equipment (Emitech K575X Sputter Coater) for 10 seconds prior to Scanning Electron Microscopy (SEM) imaging, then dispersion of the CNT fillers was examined using Philips XL30 ESEM.

CHAPTER 2: Percolation thresholds in CNT-Polymer Composites

This chapter will describe how to estimate the percolation threshold and examine it with experimental results by measuring electrical conductivity of CNT-polymer composites.

2.1 Introduction

Polymer composites containing conducting fillers[3] such as carbon black[4], carbon fiber, and metal fibers have been extensively investigated for various applications such as electromagnetic interference (EMI) shielding[5], electronic packaging[6], radar absorption[7], *etc.,* However, presently used composites require high filler to polymer loading ratios which deteriorates the overall mechanical properties, through a compromise of intrinsic matrix morphology.[8] A possible way to ameliorate the above problems, through using *low* filler volume fractions, incorporates carbon nanotubes (CNTs) in composites.[9,10,11,12] A concomitant large aspect ratio and tunable electrical conductivity would enable electrical percolation to be achieved at very small CNT volume fractions[11]. The use of small CNT volume fractions would also reduce the economic costs and clustering of the CNTs within the polymer matrix, important for large scale application. In this paper, we discuss the issue of the minimum volume fraction necessary, *i.e.,* the percolation threshold (ϕ_c) for the CNT-polymer composites to serve as electrically or thermally conductive materials through percolation theory [13].

2.2 Materials and Methods

2.2.1 Synthesis

We have sought to understand issues associated with the uniform dispersion of CNTs into polymer matrices through optimized synthesis/processing, involving enhanced nanotube-polymer interactions through chemical functionalization schemes. We chose for our initial experiments, a composite of CNTs and a Reactive Ethylene Terpolymer (RET: Elvaloy 4170) – Figure 2. 1 Both pristine and carboxyl functionalized SWNTs (average diameter 1-2 nm, and length 5-20 μm) and MWNTs (average diameter 40 nm, length 5-9 μm) were used and dispersed in toluene with sonication. The exact location of the functional groups would depend on the defect density on the nanotubes which can be

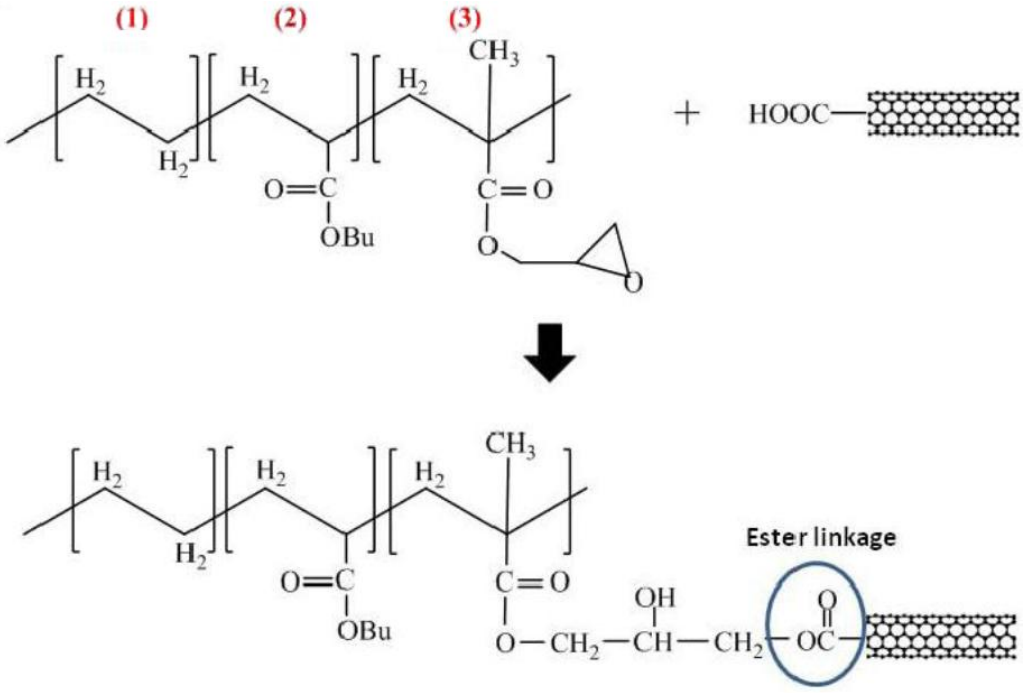

Figure 2. 1 Schematic of reaction between CNT functional groups with epoxy groups on the RET constituted from (1) polyethylene, (2) methyl-methacrylate, and (3) epoxide groups. While (1) and (2) contribute to mechanical robustness, (3) is used for forming ester linkages to –COOH groups on the CNTs for enhanced bonding and dispersion.

manipulated.[14] If the defects are randomly dispersed, isotropic bonding of the nanotubes with the polymer matrix is implied and would yield uniform dispersion and mixing. It was typically seen that sonication reduced the average length of the SWNTs to ~ 4.3 μm, with a bundle diameter ~ 4.8 nm, resulting in an aspect ratio of ~ 880. On the other hand, the MWNTs have an average length of 1.4 μm, with a bundle diameter ~ 40 nm, yielding an aspect ratio of ~ 33.

The nanotube dispersion was added to the RET solution (in toluene), and then the mixture was ultrasonicated for 5 hours. To remove excess solvent, the mixture was stirred and evacuated in vacuum (10^{-3} Torr) for 12 hours. Subsequently, a hot press was used to press the composites into the desired thickness, of ~ 2 mm, reported here.

2.2.2 Electrical conductivity measurement

The four-wire resistance method was used to measure the resistance (R) for the nanocomposites with R < 1GΩ, while for higher resistance (> 1 GΩ) composites, two point measurements using the Agilent B1500A semiconductor device analyzer, with triaxial probes were used. The composites were treated with oxygen plasma and subsequently, 5-10 nm of Ti, along with ~ 100 nm of Au were sputtered for electrical contacts.

2.2.3 Scanning electron microscopy (SEM)

The dispersion of the CNT fillers was examined using a scanning electron microscopy (SEM, Philips XL30 ESEM). The samples were gold-coated using sputter coater (Emitech K575X Sputter Coater) for 30 seconds prior to SEM imaging.

2.3 Results and Discussion

We indeed observed a *more uniform dispersion* for both *low* - Figure 2. 2 (a), *high*- Figure 2. 2 (b) COOH-SWNT filling fractions, and *high* COOH-MWNT filling fraction in Figure 2. 2 (d), as seen in the fracture surface images of the composites, in comparison to the clumped fillers observed for pristine CNT based composites in Figure 2. 2 (c).

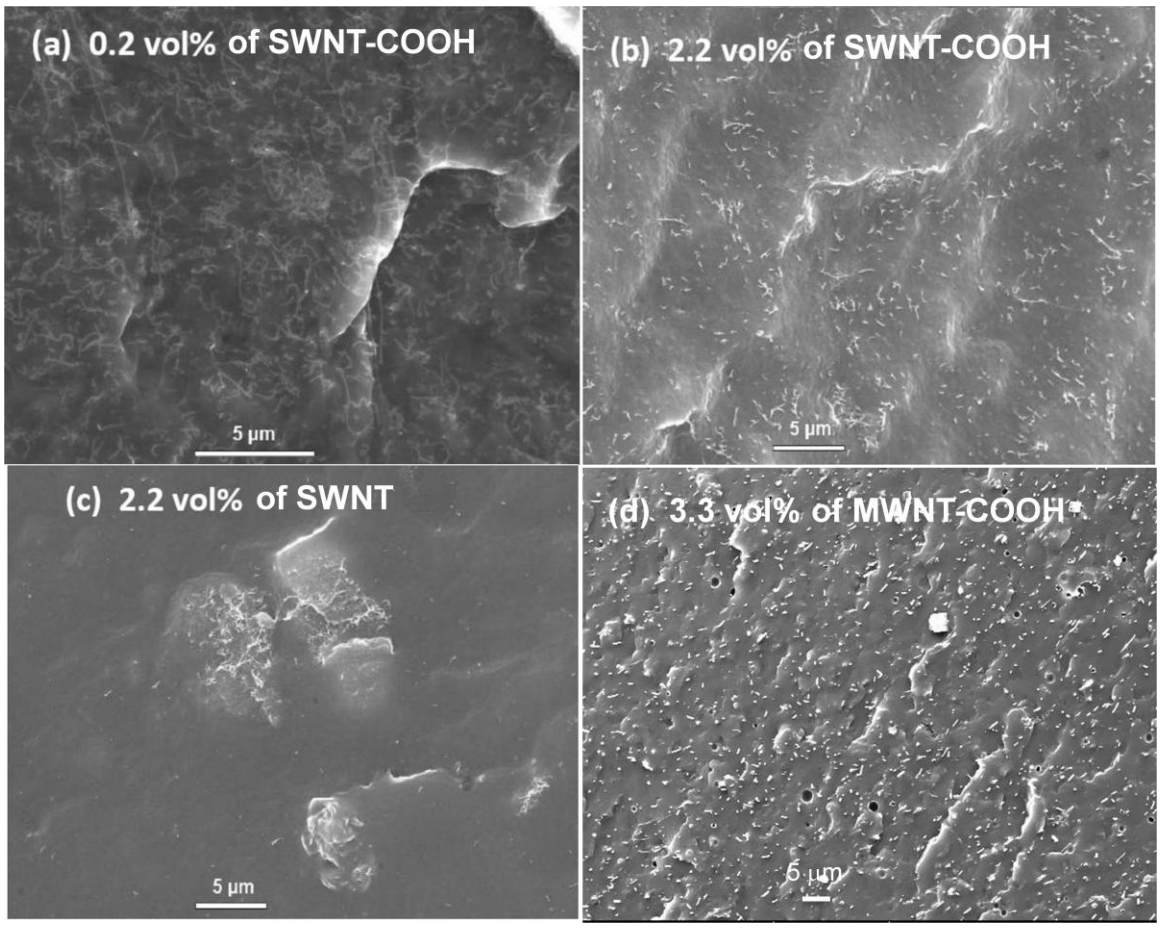

Figure 2. 2 Scanning Electron Microscope (SEM) micrographs illustrating uniform dispersion in the RET polymer at (a) 0.2, (b) 2.2 volume % functionalized SWNT, and (d) 3.3 volume % functionalized MWNT filling fractions while (c) non-functionalized SWNTs exhibit clumping.

The DC conductivity (σ_{DC}) of the polymer composites as a function of the CNT (SWNT and MWNT) filler concentration (ϕ) is shown in Figure 2. 3. It is immediately apparent that there is a much greater enhancement in the electrical conductivity (over ten orders of magnitude) compared to the approximately two-fold increase in the thermal conductivity values. The σ_{DC} were fit to the relations of the following form, where ϕ_c is the threshold volume fraction for electrical percolation, while *s* and *t* are critical exponents at the subcritical and overcritical region, respectively.

$$\sigma_{DC} \sim \begin{cases} (\phi_c - \phi)^{-s}, \phi_c < \phi \\ (\phi - \phi_c)^{t}, \ \phi > \phi_c \end{cases} \tag{1}$$

Given that the aspect ratio (*A.R.*) was ~ 880 for the SWNTs and ~ 33 for the MWNTs, the theoretical ϕ_c was calculated from excluded volume percolation theory[15], to be ~ 0.08 and ~ 1.9 vol %, respectively, using

$$\phi_c(A.R.) = \frac{1.4}{\frac{4\pi}{3}(A.R.)^3 + 2\pi(A.R.)^2 + \frac{\pi}{2}(A.R.)} \left(\frac{\pi}{6}(A.R.)^3 + \frac{\pi}{4}(A.R.)^2\right) \tag{2}$$

We have also shown how the variability in CNT lengths on the *A.R.* and the electrical percolation threshold could be dealt with through using statistical analyses[13]. Such modeling could be used to *a priori* determine the threshold and considers realistic process variability which could then be extended to other mutable CNT characteristics such as diameter, agglomeration, curvature, *etc*. Consequently, for the carbon nanotube-polymer composites, both $\phi_c < \phi$ and $\phi > \phi_c$ regimes were accessible and fit, resulting in a ϕ_c ~ 0.074 and 2.0 vol % of SWNT and MWNT filling fractions of the percolation threshold, respectively. For $\phi_c < \phi$, the *s* was ~ 0.7 for the both SWNT and MWNT based

composites, while for $\phi > \phi_c$ t was determined to be ~ 3.5 and ~ 5.2 for the SWNT and MWNT based composites, respectively.

2.4 Conclusions

We have shown that the onset of electrical conductivity in nanotube-polymer composites, as determined through the percolation thresholds, can be fitted with power law equations. The close correspondence of the experimental values to those determined from theory is quite remarkable and suggests that similar processes are operative in two widely differing phenomena. Further research should probe the relationships between the exponents, the influence of the respective conductivity contrast ratio of the fillers (nanotubes) and the matrix (polymer), *etc.* Our investigations could yield better insight into percolation phenomena, of wide importance in the theory of networks, and the optimal conditions for nanotube connectivity and dispersion for wide scale application.

2.5 Acknowledgments

This chapter, in part, is a reprint of the material as it appears in the following publication: Kim, B.-W., Pfeifer, S., Park, S.-H. & Bandaru P. R. Experimental determination of the onset of electrical and thermal conductivity percolation thresholds in carbon nanotube-polymer composites. *Mater Res Soc Symp Proc.* **1312** 2011. doi:10.1557/opl.2011.114. The dissertation author was the primary investigator and author of this paper.

CHAPTER 3: Evidence of percolation related power law behavior in the thermal conductivity of nanotube/polymer composites

This chapter shows a power law relation for the thermal conductivity, indicative of percolation, through measurements on carbon nanotube/polymer composites. Our results contradict earlier assertions and indicate that synthesis methodologies may be adapted to facilitate such behavior. Consistent modeling of the experimentally determined electrical and thermal conductivity anisotropy, in addition to the incorporation of interfacial resistance, was used to understand the underlying mechanisms and variations.

3.1 Introduction

The large length to diameter aspect ratio of one dimensional nanostructures such as carbon nanotubes (CNTs) or nanowires is advantageous for enhancing both the electrical conductivity (σ) and thermal conductivity (κ) of relatively insulating matrices, *e.g.*, polymers, at relatively low nanostructure filler fractions. Integral to such possible enhancement are (i) the postulated high conductivity of the nanostructures, along the length of the wires, due to the reduced scattering space/probability[16, 17], and (ii) that the fillers span/percolate through the matrix. Moreover, it would be expected that the anisotropy in the σ and the κ of the fillers would be transferred to the matrix and the study of concomitant effects together with aspects related thermal percolation, is discussed in this letter. Such investigations would have wide implications to a wide

variety of envisaged applications of nanostructure/polymer composites incorporating structural reinforcement[18], electromagnetic interference (EMI) shielding[3, 19], electrochemical capacitors,[20] *etc.*

3.2 Experimental Details

In this study, multi-walled CNTs (of average length 1.6 μm and diameter of 45 nm, with standard deviations of 0.5 μm and 14 nm respectively, yielding an average length/diameter aspect ratio - *A.R.*, of ~ 35) in a range of volume fractions (ϕ), *i.e.*, 1-10

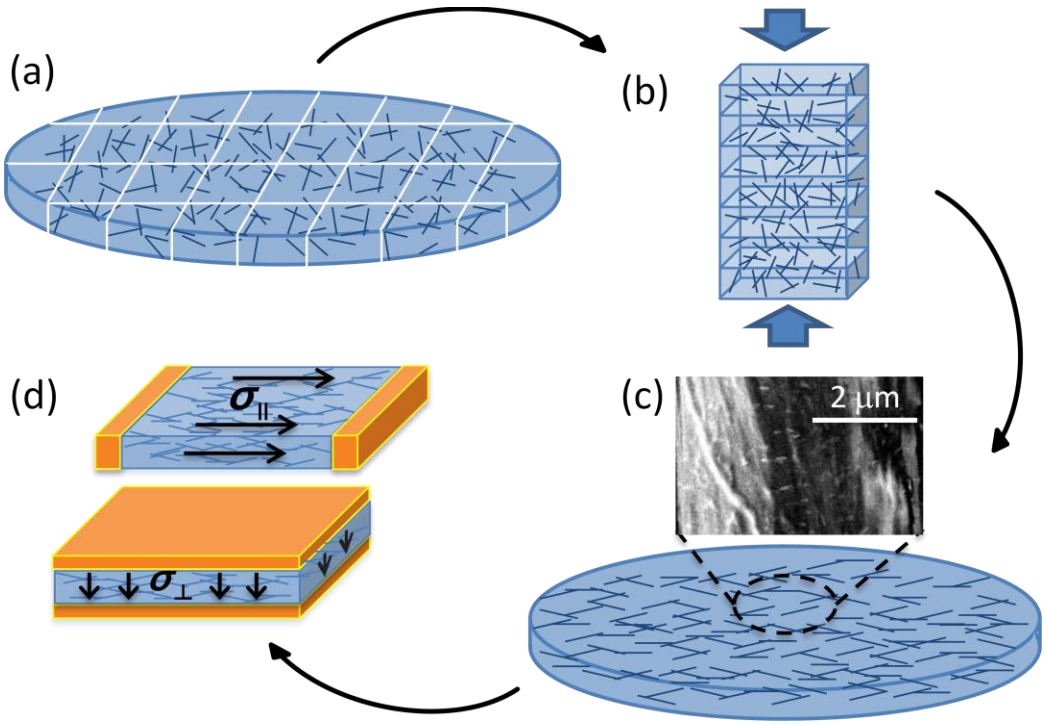

Figure 3. 1 **(a)** Blended CNT/polymer composite was diced, and **(b)** subject to repeated compressive stress. **(c)** The compressed sheet comprises CNTs preferentially aligned in the plane of the sheet. **(d)** *In-plane* (top) *and cross-plane* (bottom) electrical and thermal conductivity measurements were carried out to ascertain anisotropy and percolation.

volume % (higher fractions rendered the composites brittle) were dispersed uniformly in a reactive ethylene terpolymer (RET) matrix through a careful blend of solution processing and mixing techniques over – as outlined in Figure 3. 1.

The uniformity of the dispersion was gauged through (a) considering the nanostructure dispersion, through scanning electron microscopy (SEM) micrographs at various length scales (1 μm – 100 μm), as well as through (b) our development and use of a image processing algorithm for comparing the given distribution to a preferred (*e.g.*, uniform) distribution[21]. The underlying rationale for the choice of the RET was that ester bond linkages between the carboxyl groups on acid functionalized CNTs and the epoxide groups on the polymer would enable robust bonding, as was verified through Fourier transform infrared spectroscopy (FTIR)[5]. Consequently, both functionalized CNTs and RET were solubilized in toluene solvent and blended through ultrasonication. The blend was cast into a glass Petri dish, where the excess solvent was removed by heat treatment in a furnace - further details of the composite synthesis technique have been previously published[22]. The obtained composite was removed from the dish and then stacked and subject to a hot press treatment to obtain CNT/RET films of the desired thickness. We report electrical and thermal measurements on representative composite films of 2 mm thickness.

Four probe measurements were used for the σ (= x/RA, evaluated from the measured electrical resistance R, with x as the contact spacing and A as the cross-sectional area) of the composites with $R < 1$ GΩ, while for higher resistance composites two-point measurements (using the Agilent B1500A semiconductor device analyzer, with triaxial probes) were employed. The composites were subject to mild oxygen plasma

treatment to remove surface contamination and subsequently, 5-10 nm of Ti followed by 100 nm of Au were sputtered on for electrical contacts. For measurements of the *in-plane* conductivity ($\sigma_{\parallel}$) the contacts were on the *either side* of the composite, while measurements of the *cross-plane* (/through thickness) conductivity ($\sigma_{\perp}$) used contacts deposited on the *top* and *bottom* of the composite – see Figure 3. 1(d). Self-heating was negligible due to the low applied power.

3.3 Results and Modeling

The measured $\sigma_{\parallel}$ and $\sigma_{\perp}$ as a function of the CNT concentration is plotted in Figure 3. 2. The variation of both $\sigma_{\parallel}$ and $\sigma_{\perp}$ could be fitted to power law relations of the form[13]:

$$\sigma_{DC} \sim \begin{cases} (\phi_c - \phi)^{-s}, \phi_c < \phi \\ (\phi - \phi_c)^{t}, \ \phi > \phi_c \end{cases} \tag{1}$$

where ϕ_c is the threshold volume fraction for electrical percolation, while *s* and *t* are critical exponents. We estimated, from excluded volume percolation theory[15, 23], that for CNTs with an aspect ratio (*A.R.*) of ~ 35, and using:

$$\phi_c(A.R.) = \frac{C}{\frac{4\pi}{3} + 2\pi(A.R.) + \frac{\pi}{2}(A.R.)^2}\left[\frac{\pi}{6} + \frac{\pi}{4}(A.R.)\right] \tag{2}$$

C is a constant in the range of 1.4 (for thin rods) to 2.8 (for spherical objects)[24]. Using *C* ~ 1.4, for the nanotubes, a ϕ_c of ~ 2.2 volume % was estimated. While the fitted ϕ_c was ~ 2.3 vol% for the $\sigma_{\parallel}$ change, a value of ~ 3.3 volume % was noted for the $\sigma_{\perp}$ variation. Moreover, there was a more gradual (*t* ~ 4.2 for $\sigma_{\perp}$ compared with a *t* value ~ 5.7 for the

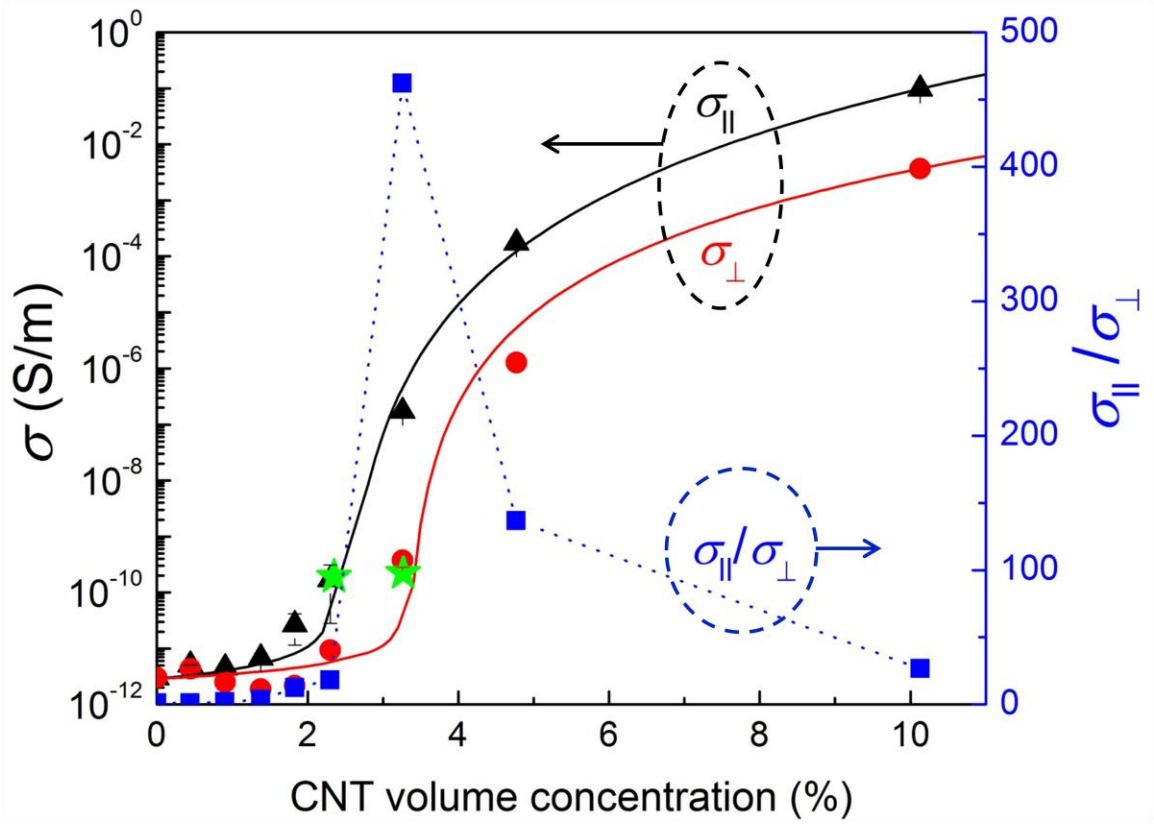

Figure 3. 2 The variation of the measured electrical conductivity with added CNT filler concentration depicted for the *in plane* (σ_{II}) and *cross plane* ($\sigma_{\perp}$) configurations. The anisotropy ratio, *i.e.*, $\sigma_{II}/\sigma_{\perp}$ is indicated on the right hand axis. The * indicates the results of the Straley model (see text) relating the product of the *electrical* resistances of the matrix and the filler to the percolation threshold.

σ_{II} variation[25]) and smaller net increase. The differing values of ϕ_c for the $\sigma_{\perp}$ and σ_{II} indicate anisotropy and the $\sigma_{II}/\sigma_{\perp}$ ratio has been indicated in Figure 3. 2, *e.g.*, the larger value for $\sigma_{\perp}$ could be tentatively understood from the greater deviation from isotropic arrangement[26, 27] of the nanotubes.

Concomitantly, the *cross plane* ($\kappa_{\perp}$) and *in-plane* (κ_{II}) thermal conductivity values were estimated through a steady state method and the 3ω methology[2],

respectively. For $\kappa_{\perp}$ the experimental apparatus was modeled and constructed in accordance with ASTM (American Society for Testing and Materials) standards E1225 and D 5470. The accuracy of measurement was estimated to be ~ 3% through comparison with standards. For the $\kappa_{\parallel}$ measurements, employing the 3ω technique, Ti/Au metal lines (70 μm wide and 10 mm long) which serve as both heater and thermometer were deposited on the composites, with the length scales chosen so as to approximate a narrow line heat source[28, 29] (with a ratio of the sample thickness to the metal line width of ~30). Using a lock-in amplifier (Stanford Research Systems: SR 830) and a Wheatstone bridge setup, alternating current, $I(\omega)$, of angular frequency ω (in the range of 0.1 Hz-1000 Hz), passed through the metal lines induces resistance oscillations at 2ω: $R(2\omega)$, due to Joule heating (~ I^2R), from which the thermal conductivity can be deduced from the third harmonic voltage, $V(3\omega)$ (= $I(\omega)R(2\omega)$). The temperature change (ΔT) was deduced using the relation[2]: $\Delta T = \frac{2V(3\omega)}{\alpha V(\omega)}$, where α is the measured temperature coefficient of resistance of the metal line. Assuming an adiabatic boundary condition at the bottom of the composite (which is valid for a thermal penetration depth smaller than 2 mm[29]) the estimated ΔT could be then related to the thermal conductivity product, $\kappa_{\parallel} \cdot \kappa_{\perp}$, obtained through:

$$\Delta T \cong \frac{P}{2\pi\sqrt{\kappa_{\parallel} \cdot \kappa_{\perp}}}\left[-\ln(\omega) + G\right] \qquad (3)$$

In (3), P is the electrical power per unit length of the heater and G is a constant. Combining the steady-state and the 3ω measurements, the individual values of $\kappa_{\parallel}$ and $\kappa_{\perp}$ were computed.

The measured $\kappa_{\perp}$ and the estimated $\kappa_{\parallel}$ are then plotted as a function of the CNT concentration in Figure 3. 3 along with the $\kappa_{\parallel}/\kappa_{\perp}$ anisotropy ratio. While a fairly linear change was noted for $\kappa_{\perp}$, a percolation like behavior, similar to the variation in σ, was observed in $\kappa_{\parallel}$. We then attempted to fit the $\kappa_{\parallel}$ variation using expressions of the form:

$$\kappa_{\parallel} \sim \begin{cases} (\phi_{c,k} - \phi)^{-p}, \phi_{c,k} < \phi \\ (\phi - \phi_{c,k})^{q}, \ \phi > \phi_{c,k} \end{cases} \quad (4)$$

Where, $\phi_{c,k}$ is now the threshold volume fraction for the onset of thermal percolation, and p and q are critical exponents in the respective regimes. We obtained, experimentally, a $\phi_{c,k}$ ~2.2 vol %, close to the theoretically expected value, with p ~ 0.2 and q ~ 0.1. The value of the exponents in the power laws depends on the particular type of conductivity[25, 30] (*i.e.*, electrical or thermal) as well as on the ratio of the respective conductivities of the constituent phases[31].

The concomitant larger variation in the increase of the σ (ten-twelve orders of magnitude for $\sigma_{\perp}$ and $\sigma_{\parallel}$) of the CNT/polymer composites compared to the increase of the κ (50% and 400% for $\kappa_{\perp}$ and $\kappa_{\parallel}$, respectively) may be attributed to the intrinsically greater range in electrical conductivity. In the former case, one has to consider the much lower electrical resistance of the CNTs compared to the polymers while there is generally a much smaller variation in κ between disparate materials. The substantial enhancement in $\kappa_{\parallel}$ compared to $\kappa_{\perp}$ is also to be noted. We ascribe the $\kappa_{\parallel}$ increase to the effects of percolation. Further evidence was obtained through adapting a Straley model[32] (used for determining the critical exponents for the conductivity of random resistor lattices), where the filler (R_f) and matrix (R_m) could be represented as *thermal* resistors. Through such

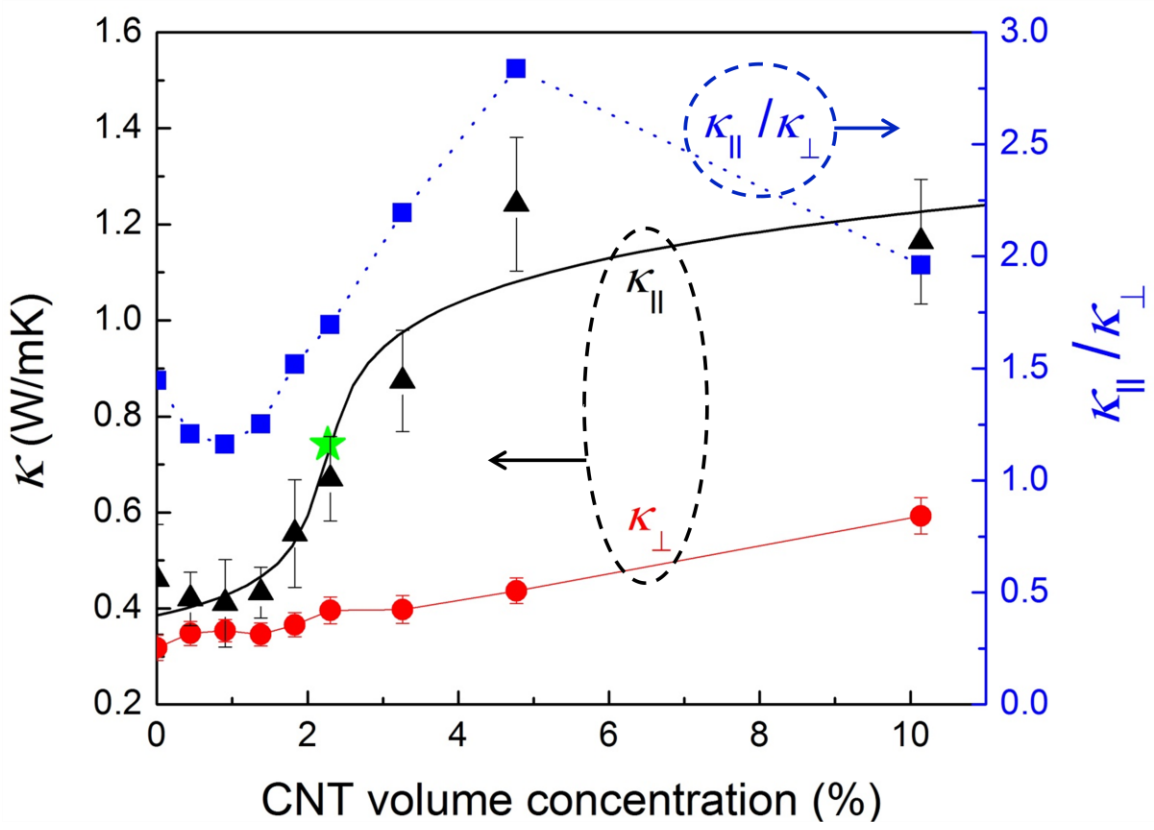

Figure 3. 3 The variation of the measured thermal conductivity with added CNT filler concentration depicted for the *in plane* ($\kappa_{||}$) and *cross plane* ($\kappa_{\perp}$) configurations. The anisotropy ratio, *i.e.*, $\kappa_{||}/\kappa_{\perp}$ is indicated on the right hand axis. The * indicates the results of the Straley model (see text) relating the product of the *thermal* resistances of the matrix and the filler to the percolation threshold.

modeling, the effective thermal conductivity at the percolation threshold fraction could be related to $R_f^u R_m^{1-u}$, where $u = p/(p+q)$, and the estimated value has been indicated through a * in Figure 3. 3 The equivalent σ values, where the filler and the matrix were represented as *electrical* resistors have been indicated, through * in Figure 3. 2.

We model such connectivity effects encompassing *both* electrical and thermal conductivity through considering the total number of percolating networks in the *in plane*

and *cross plane* directions, contributing to an equivalent resistance, $R_{\parallel}$ and $R_{\perp}$ respectively. Following the schematic in Figure 3. 4, we assume that each network is comprised of a series of nanotubes, and many such networks yield a nanostructure contributed total resistance in the *in-plane* direction ($R_{CNT,\parallel}$). Conduction would occur simultaneously through the polymer matrix of resistance = $R_{M,\parallel}$. If the resistance of a

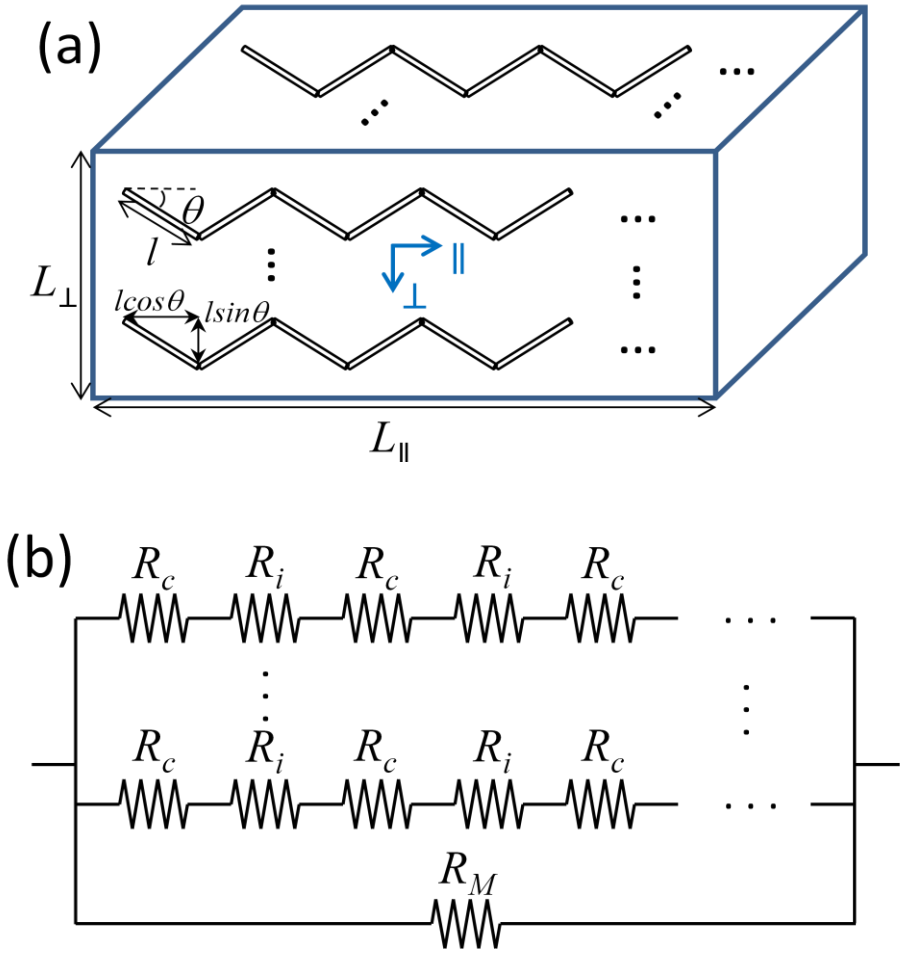

Figure 3. 4 (a) Modeling networks of aligned MWCNTs in the polymer matrix, and (b) the equivalent electrical/thermal circuit schematic with R_c as the nanotube resistance and R_i as the interfacial resistance.

single nanotube, $R_c = \frac{l}{A_c \sigma_c}$, with l being the average nanotube length, A_c as the cross-sectional area, and σ_c the conductivity (which should now be interpreted as an electrical: σ, *or* thermal conductivity: κ) with an interfacial resistance, R_i (in units of $\Omega\,m^2$), then $R_{CNT,\parallel}$ would be:

$$\frac{1}{R_{CNT,\parallel}} = \frac{1}{\left(R_c + \frac{R_i \cos(\theta)}{A_c}\right)\frac{L_\parallel}{l\cos(\theta)}} \frac{N_C l \cos(\theta)}{L_\parallel} \tag{5}$$

θ is an average orientation angle between the CNT longitudinal axis and the horizontal, $L_{||}$ is the length of the composite sample, and N_c indicates the total number of CNTs and estimated through the incorporated volume fraction (ϕ). The second multiplicative term on the right is a measure of the number of horizontal networks. The $R_{M,\parallel} = \frac{L_\parallel}{A_\parallel (1-\phi)\sigma_m}$, where $A_\parallel$ is the composite cross-sectional area and σ_m is the matrix (/polymer) conductivity. The *net in-plane* conductivity ($\sigma_\parallel$) constituted of $R_{CNT,\parallel}$ and $R_{M,\parallel}$ would be:

$$\sigma_\parallel = \frac{\phi \cos^2(\theta)}{\left(\frac{1}{\sigma_c} + \frac{R_i \cos(\theta)}{l}\right)} + (1-\phi)\sigma_m \tag{6}$$

Through similar methodology, the *net cross-plane* conductivity ($\sigma_\perp$) constituted of $R_{CNT,\perp}$ and $R_{M,\perp}$ would be:

$$\sigma_\perp = \frac{\phi \sin^2(\theta)}{\left(\frac{1}{\sigma_c} + \frac{R_i \sin(\theta)}{l}\right)} + (1-\phi)\sigma_m \tag{7}$$

Assuming a range of θ (*i.e.*, $|\theta| < \theta_b$) and a constraint on the anisotropy ratio between the *in-plane* and the *cross-plane* conductivity, *i.e.*, $\frac{<\sigma_{\parallel}>}{<\sigma_{\perp}>} \rightarrow 1$,as $\theta_b \rightarrow \pi/2$, we derive:

$$\frac{<\sigma_{\parallel}>}{<\sigma_{\perp}>} = \frac{\theta_b + \sin(\theta_b)\cos(\theta_b) + \left(\frac{1-\phi}{\phi}\right)\left(\frac{1}{\sigma_c} + \frac{2R_i \sin(\theta_b)}{l}\right)\sigma_m}{\theta_b - \sin(\theta_b)\cos(\theta_b) + \left(\frac{1-\phi}{\phi}\right)\left(\frac{1}{\sigma_c} + \frac{2R_i \sin(\theta_b)}{l}\right)\sigma_m} \tag{8}$$

In the case of electrical conductivity, due to the measured small σ_m (~$3\cdot10^{-12}\,\Omega^{-1}\mathrm{m}^{-1}$) we could ignore the expressions on the far right hand side of the numerator and denominator, whence we obtain:

$$\frac{<\sigma_{\parallel}>}{<\sigma_{\perp}>} \cong \frac{\theta_b + \sin(\theta_b)\cos(\theta_b)}{\theta_b - \sin(\theta_b)\cos(\theta_b)} \tag{9}$$

Inserting the corresponding $\sigma_{\perp}$ and $\sigma_{\shortparallel}$ from Figure 3. 2**,** at $\phi > \phi_c$ (*i.e.*, at 3.3 vol%, 4.8 vol%, and 10 vol %), we find the θ_b values as 4.6°, 8.5°, and 19° respectively. These values were then used for interpreting the thermal conductivity variation *vis-à-vis* the percolation like behavior of $\kappa_{\shortparallel}$.

However, for modeling the thermal conductivity anisotropy, $\frac{<\kappa_{\parallel}>}{<\kappa_{\perp}>}$ the matrix conductivity, κ_m (~ 0.3 W/mK) cannot be neglected, and terms involving the thermal interfacial resistance (R_i^{th} in units of m^2K/W) would remain:

$$\frac{<\kappa_{\parallel}>}{<\kappa_{\perp}>} = \frac{\theta_b + \sin(\theta_b)\cos(\theta_b) + \left(\frac{1-\phi}{\phi}\right)\left(\frac{1}{\kappa_c} + \frac{2R_i^{th} \sin(\theta_b)}{l}\right)\kappa_m}{\theta_b - \sin(\theta_b)\cos(\theta_b) + \left(\frac{1-\phi}{\phi}\right)\left(\frac{1}{\kappa_c} + \frac{2R_i^{th} \sin(\theta_b)}{l}\right)\kappa_m} \tag{10}$$

Along with the corresponding $\kappa_{\parallel}$ and $\kappa_{\perp}$ from Figure 3. 3, the θ_b values obtained previously were inserted into (10), to consistently estimate a κ_c (~ 240 W/mK) and an R_i^{th} (~ $7 \cdot 10^{-8}$ m^2K/W). Such estimates are in excellent accord with previous evaluations of nanotube interfacial thermal resistance[33] and further indicate a significant modulation of the thermal conductivity of nanostructures when they are dispersed into a matrix. While previous reports[34, 35] indicated a lack of percolation due to (i) the relatively low thermal conductivity contrast and (ii) the interfacial resistance between the conducting nanostructure and the matrix (polymer), we have then seen that such characteristics are indeed possible. In such previous studies, *e.g.,* it was concluded based on theoretical analysis (based on the finite element method: FEM and molecular dynamics) that the low thermal conductivity contrast (of less than 10^4) between the matrix and the filler precludes percolation. A linear variation of the thermal conductivity with volume fraction was predicted based on effective medium theory, which may not be valid at/near to the percolation threshold[13, 37]. Single walled nanotube-epoxy composites were studied[35] where the random orientation of the nanotubes was thought to be the reason for the thermal conductivity increase. Indeed, a greater degree of isotropy would imply a lower percolation threshold as was indicated in Figure 3. 2. Additionally, previous work[35, 36] did not consider the effects of interfacial resistance between the nanotubes and the matrix, the effects of which have been discussed in much more detail in this paper.

3.4 Conclusions

We have then shown that it is feasible to adapt a synthesis methodology, *e.g.*, using stacking of nanotube/polymer composite sheets, facilitating such behavior. We surmise that an increased nanotube aspect ratio, enhanced from that presented in this paper, would yield a corresponding exponential increase of the thermal conductivity.

In summary, we have shown, through detailed experiments and modeling, evidence of anisotropy in both the electrical and thermal conductivity in nanotube/polymer composites. A power law relation for the thermal conductivity has been indicated with implications for tunable thermal conductivity and thermal switching.

3.5 Acknowledgments

This chapter, in full, is a reprint of the material as it appears in Kim, B.-W., Park, S.-H., Kapadia, R. S. & Bandaru, P. R. Evidence of percolation related power law behavior in the thermal conductivity of nanotube/polymer composite. *Appl Phys Lett*. **102** 243105 (2013). The dissertation author was the primary investigator and author of this paper.

CHAPTER 4: Anomalous variation of the specific heat capacity at the electrical and thermal percolation threshold in nanotube/polymer composites

This chapter shows anomalous variation in the measured specific heat capacity of nanocomposites based on extensive calibration and characterization (through two independent methodologies). The crystalline order (determined through x-ray diffraction methods) was found to be anti-correlated to the specific heat and hinted that the underlying arrangement of nanotubes in the polymer matrix could be responsible for such change. We interpreted the decrease in terms of the partition of the total number of nanostructures into isolated or clustered/connected entities and the consequent modulation of the entropic characteristics as well as the conductivity.

4.1 Introduction

The placement of nanostructure fillers in polymers, in addition to the technological value[38], yields significant insights into material interactions and consequent physical and chemical property modulation. A related aspect concerns the widespread use of carbon nanotube (CNT) additives in battery electrodes and polymers for composite synthesis[39,40] based on the advantages of a large length to diameter aspect ratio (*A.R.*). Consequently, a significant change of the composite character at relatively low (< 0.01 wt%) nanotube filler concentrations may then be obtained. A significant underlying mechanism for the drastic change is the encompassing of the polymer matrix, through the percolation[13, 41] of the nanotubes, which has been shown to modulate the mechanical

characteristics[42] as well as significantly modulate the electrical[43,44] and thermal conductivity[45] attributes of the polymer. Here, we report an unusual specific heat variation in nanotube/polymer composites, related to a reduction in its value at the electrical and the thermal percolation threshold, with a concomitant increase in the crystallinity.

4.2 Electrical and thermal conductivity percolation

In this study, multi-walled CNTs of *A.R.* ~ 35 (estimated through the ratio of the average length 1.6 μm and diameter of 45 nm - with a standard deviation of 0.5 μm and 14 nm, respectively) were uniformly dispersed into a RET (reactive ethylene terpolymer) matrix in a volume fraction (ϕ) range of 0.004 to 0.1. The upper limit of ϕ was dictated by the mechanical stability of the composites, as it was found that higher ϕ made the samples brittle. The dispersion homogeneity was monitored through scanning electron microscopy (SEM) micrographs and quantified through our development of an image-processing algorithm, which allowed the comparison of the obtained uniformity with that of a preferred pattern[46]. The rationale for the choice of the RET and further details on the processing have been previously reported[5]. The electrical conductivity (σ) of the composites (with sputtered Ti (5 nm)/Au (100 nm) as contacts) with electrical resistance, *Rel* < 1 GΩ) was measured through standard four-probe measurements while for composites with *Rel* > 1 GΩ, two-point methods were employed (using the Agilent 1500A semiconductor device analyzer, with triaxial probes). The results, shown in Figure 4.1 indicate a percolation-like behavior with a ten-order of magnitude change in the σ

with increasing ϕ. We predicted[23,43] a value of 0.021 for the percolation threshold volume fraction (ϕ_c) – per Eqn. (1) below, using for the constant B a value of 1.4, appropriate for thin rods.[24]

$$\phi_c(A.R.) = \frac{C}{\frac{4\pi}{3} + 2\pi(A.R.) + \frac{\pi}{2}(A.R.)^2}\left[\frac{\pi}{6} + \frac{\pi}{4}(A.R.)\right] \quad (1)$$

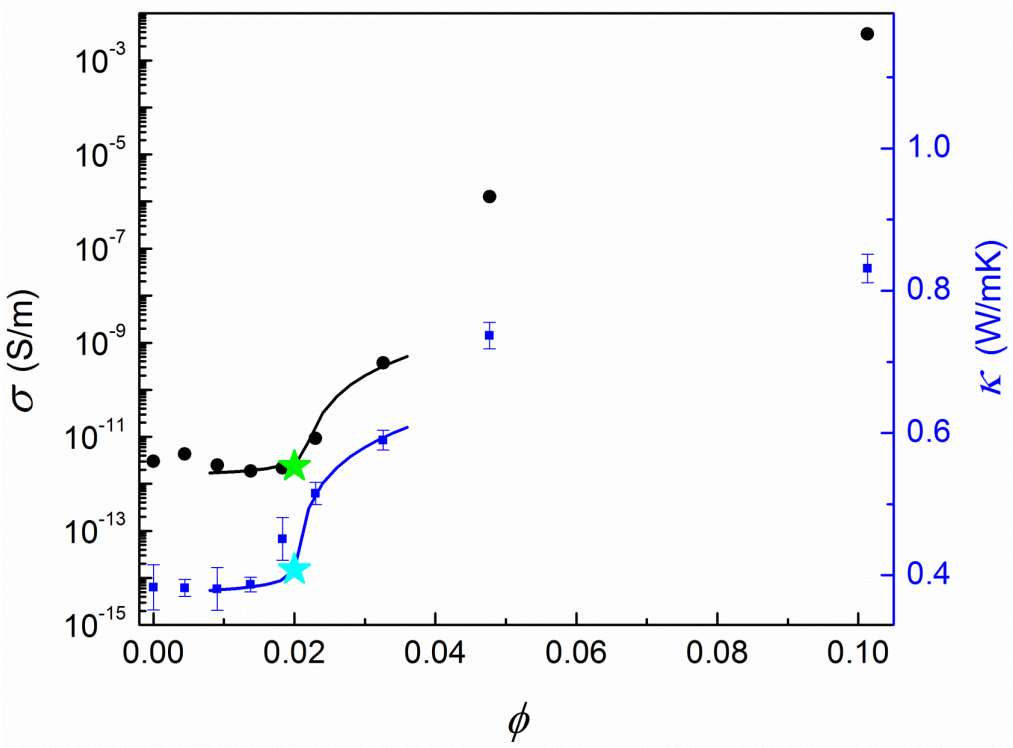

Figure 4. 1 Electrical and thermal conductivity percolation in the nanocomposites. The measured electrical conductivity (σ): left vertical axis, and thermal conductivity (κ): right vertical axis, as a function of the nanotube filler fraction (ϕ). The solid lines are fits to the conductivity variation near the percolation threshold (ϕ_c ~0.02) to a power law expression of the form: $\sigma \sim |\phi - \phi_c|^t$, where t is a critical exponent.

A ϕ_c of ~ 0.02 was experimentally estimated through fitting the conductivity variation, close31 to ϕ_c, to a power law expression of the form: $\sigma \sim |\phi - \phi_c|^t$, where *t* is a critical exponent[13, 25]. While the threshold could depend on microscopic details, the *t* is material independent and universal[47] at *t* = 2, as was indeed found through our observations and fitting.

4. 3 Decrease of specific heat capacity at the percolation threshold

Concomitantly, we measured thermal conductivity (*k*) of the polymer nanocomposites through both a 3ω based methodology[2] and steady state methods. It was seen that k variation with ϕ also followed a percolation-like transition, and was fitted to a power law expression with a similar ϕ_c of ~ albeit with a different exponent, *t* of ~ 0.3. The difference in the *t* from the value obtained from the electrical conductivity measurements was ascribed to the substantial influence of the interfacial resistance9 as well as the different physical origin of thermal transport[25,31]. In both the electrical and thermal measurements, it was ensured that the sample and the metal lines were electrically isolated/ mutually insulated at all CNT concentrations through monitoring the electrical capacitance. While the traditional use of the 3ω method, with reference to the measured third harmonic of the voltage *V* (3ω), at a given angular frequency ω (= 2πf, where *f* is the measurement frequency) - due to the product of the alternating current: *I* (ω) and the Joule heating induced resistance variation: *R* (2ω), has been in the measurement of the κ, we coopted the underlying principles for the measurement of the specific heat capacity: C_p, of the composites. It was previously shown that[2]:

$$V(3\omega) = \frac{[V(\omega)]^3}{\kappa 2\pi l R_m^2}\frac{dR_m}{dT}\int_0^\infty \frac{sin^2(kb)}{(kb)^2\sqrt{k^2+2\omega\rho C_p/\kappa}}dk \quad (2)$$

For our measurements, l (= 10 mm) and $2b$ (=70 μm) refer to the length and width of the metal (*me*) line, which served as both the heater and thermometer and were chosen so as to approximate a narrow line heat source (with a ratio of the sample thickness to the metal line width of ~ 30). The density (ρ), resistance of the metal line (R_{me}) as well as the related temperature coefficient ($=dR_{me}/dT$) was measured and well calibrated. The variation of the V (3ω) over a range of f (from 0.1 Hz to 1000 Hz) was measured using a lock-in amplifier (Stanford Research Systems: SRS 830) in concert with a Wheatstone bridge setup (used to cancel the lower voltage harmonics). In a lower range of frequencies (from 1 Hz to 100 Hz), the slope of the $V(3\omega)$ *vs. ln* (f) was used to deduce the κ variation, with P/l as the power per unit length at 2ω. Subsequently, with the obtained values of κ for a given ϕ, the C_p was obtained through a numerical solution of Eqn. (2) and a fit to the entire curve: see inset to Figure 4. 2(a). The results of the C_p variation for a range of ϕ in the nanotube/polymer samples are indicated, through *diamond* symbols, in Figure 4. 2(a). The accuracy of measurement was estimated to be ~3 % through comparison with standards[45]. It was noted that the observed variation was unusual in that there seemed to be a dip in the C_p magnitude close to/at the ϕ_c.

As such variation was reproducible in three sets of samples, further confirmation was attempted through another independent technique. Consequently, the C_p was measured through monitoring the decay of the temperature (T) profile developed in

response to the application of electrical power pulses to sputtered Ti (10 nm)/Au (100 nm) contacts on the top and bottom of the nanocomposite sample– Figure 4. 2(b). We

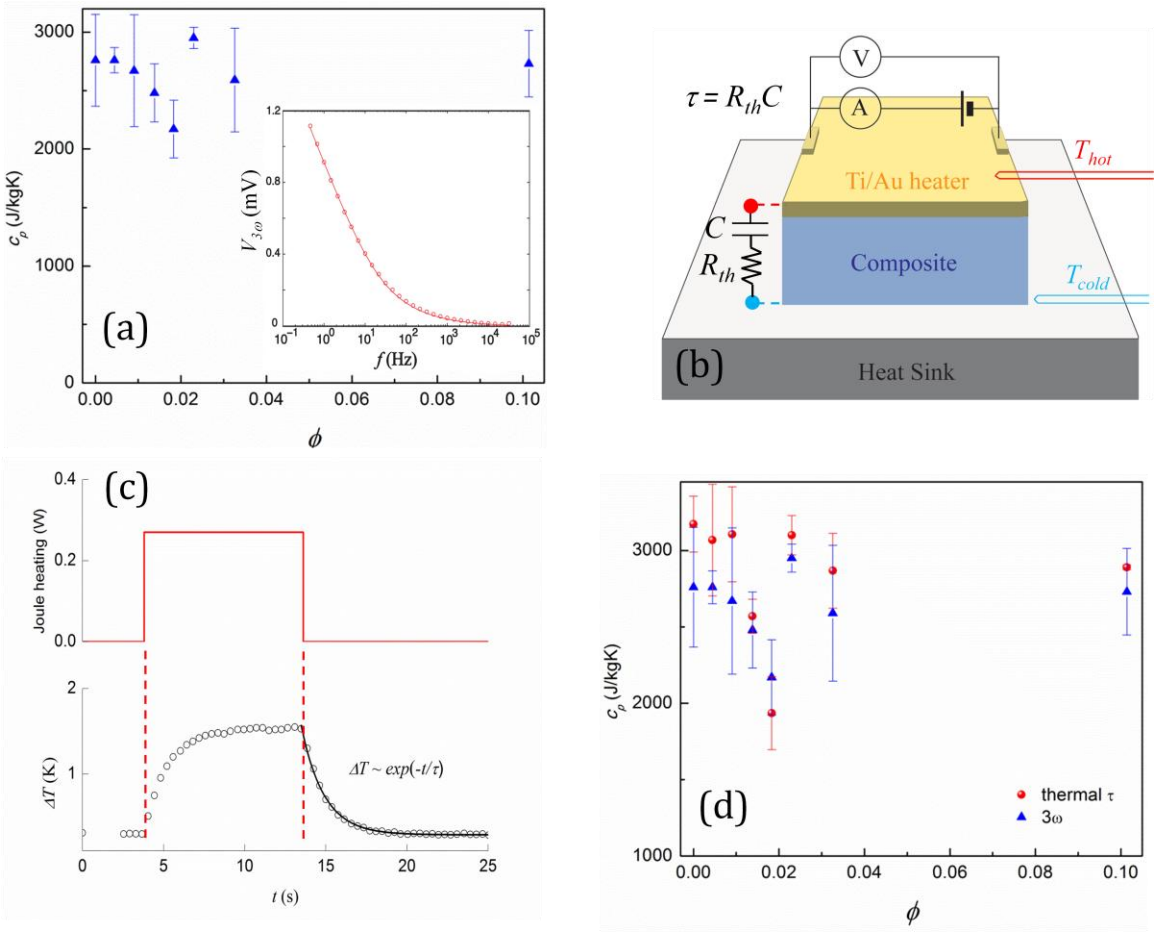

Figure 4. 2 A characteristic decrease of the specific heat capacity (C_p) at the electrical and thermal percolation threshold. (a) The variation of the C_p with ϕ, as measured by the 3ω method indicated a decrease near the ϕ_c. The *inset* shoes the measured V (3ω), at a given operating frequency (f). (b) Schematic of a thermal time constant based method for the determination of the *Cp* of the composite sample, where the temperature decay time constant $\tau = R_{th} \cdot C$ denotes the equivalent thermal resistance (R_{th}) and capacitance ($C = m \cdot C_p$, with m as the mass of the sample) measured through a (c) fit to the thermal profile (*bottom*) developed in response to an application of a power pulse (*top*) to the Ti/Au electrodes. (d) Superposed values of C_p determined through both the 3ω and the thermal time constant based measurements clearly show a dip near ϕ_c.

defined and measured a thermal time constant (τ), as the time during which the T of the sample decays by a factor of e (the base of the natural logarithm) from the profiles: Figure 4. 2(c). From the relation, $\tau = R_{th}C = R_{th} \cdot m \cdot C_p$, with R_{th} ($=\Delta T/P$, the ratio of the temperature drop: ΔT, across the sample to the applied power: P) as the thermal resistance, and C being the thermal capacitance (= the product of the mass of the sample: m and the C_p) the specific heat capacity was estimated[48]. The method was calibrated through testing for the C_p of a variety of materials, *e.g.*, Pyrex glass (measured C_p = 760 J/kg·K *vs.* reported value of 750 J/kg·K[49]) and typically yielded C_p values to within 2 % of those reported in literature. The previously observed decrease in the C_p values was again observed, further enhancing our confidence that the characteristic at the ϕ_c was indeed typical to the nanotube/polymer composites. The combined data sets from both the (a) 3ω methodology, and (b) the heat pulse method measurements are indicated in Figure 4. 2(d).

We sought to understand such an unexpected change in the C_p through further diagnostics on the samples using x-ray diffraction (employing the Bruker D8, operated at 40 kV, 200 mA). A corresponding degree of crystalline order (defined for polymeric materials through the ratio of the integrated intensity of the crystalline peak to that of the amorphous background[50]) *opposite* to that observed in the C_p was revealed (Figure 4. 3) and hinted that the underlying arrangement of the nanotubes in the polymer matrix could be responsible for the specific heat variation. It has also previously been discussed, in the context of ethylene based polymers akin to RET, that an increasing crystallinity decreases the specific heat[51, 52]. The indexing of the peak positions (inset to Figure 4. 3) was done to within close accord of the published patterns[53]. The change in the XRD patterns with

increasing ϕ has been indicated in the Supplementary Information. It was intriguing to consider the notion that crystallinity seems to be maximal at the nanotube percolation threshold in the polymer. While such a correlation has been previously noted for semiconductor based systems[54], such as phosphorus doped Si:F:H alloys[55], our work is a seminal report of such phenomena in nanostructure-polymer systems. The estimated degree of crystallinity of ~ 0.27: Figure 4. 3, at the ϕ_c was intermediate to the theoretical boundary values[56] of 0.15 and 0.44 for three- and two-dimensional percolating systems and indicate a tendency towards rod-like percolation[57], as would be expected for nanotube containing systems.

Since ϕ_c indicates a degree of ordering, we attempted to relate a change in the entropy to the observed C_p variation. We hypothesized that the relative arrangement of the CNTs would determine the change as either individual entities (as at $\phi < \phi_c$) or clusters (typical at $\phi > \phi_c$). As it was previously discussed, through Figure 4. 3, that a maximum of the degree of crystallinity corresponded to the ϕ_c, it was plausible that the connectivity of the nanotubes could be related to the observed C_p. minimum. We consider the equivalence between the change of the specific heat to the change of the Boltzmann entropy (ΔS), at a given temperature[58]. The ΔS term incorporates the total number of CNTs (N_t) partitioned either into individual/isolated (Ni) or connected (Nc) constituents, *i.e.*, $N_t = N_i + N_c$, and would be proportional to $ln\ [N_t!\ /(N_i!\ N_c!)]$. The argument of the logarithm would be related to the variety of possible arrangements of the N_t ($= \phi \cdot V_s / V_{CNT}$, where V_s and V_{CNT} represent the sample volume and that of an individual CNT assumed to be a cylinder with mean length of 1.6 μm and diameter of 45 nm, respectively)

nanostructures. We consequently computed the ratio of the experimentally determined specific heat values at two particular measured values of ϕ (say, ϕ_1 and ϕ_2), *i.e.*, as $C_{p,\phi 1}$ and $C_{p,\,\phi 2}$, referenced to the value for the polymer alone, *i.e.*, $C_{p,\,\phi=0}$, through:

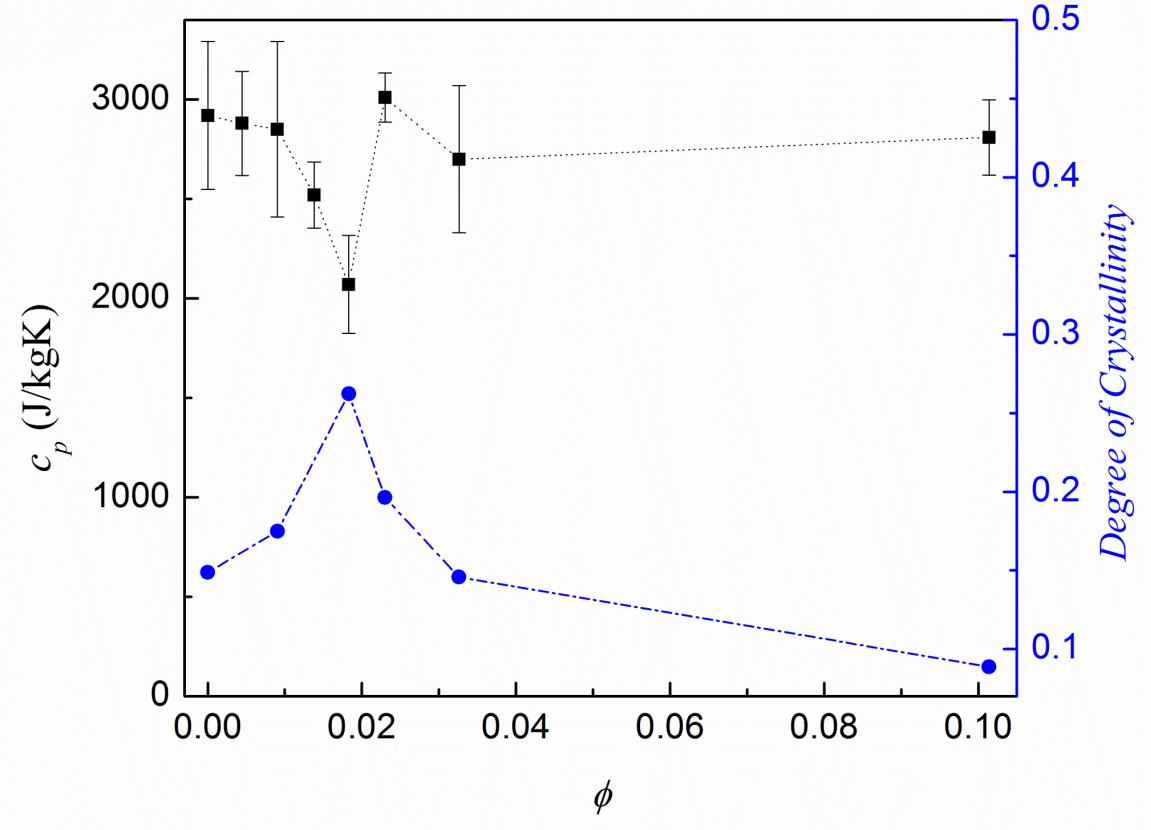

Figure 4. 3 Correlation of the measured specific heat capacity (C_p) to the crystallinity of the nanocomposite. The C_p (*left axis*) variation is anti-correlated to the change of the degree of crystalline order – determined *via* x-ray diffraction, (*right axis*) with ϕ. The *inset* indicates a typical x-ray diffractogram of the nanocomposite (for ϕ = 0.009) – indicating the Intensity (in arbitrary units, a.u.) *vs.* 2θ and the crystal plane indices above the peaks, based on which the crystallinity (defined through the ratio of the integrated intensity of the crystalline peaks: *solid* to that of the total integrated area: crystalline peak + amorphous background: *diagonal shaded*) was determined.

$$\frac{(C_{p,\phi_1}-C_{p,\phi=0})}{(C_{p,\phi_2}-C_{p,\phi=0})}=\frac{ln\left[\frac{N_{t,\phi_1}!}{N_{c,\phi_1}!\left(N_{t,\phi_1}-N_{c,\phi_1}\right)!}\right]}{ln\left[\frac{N_{t,\phi_2}!}{N_{c,\phi_2}!\left(N_{t,\phi_2}-N_{c,\phi_2}\right)!}\right]} \quad (3)$$

As the corresponding total number of nanotubes: $N_{t,\,\phi 1}$ and $N_{t,\,\phi 2}$ at ϕ_1 and ϕ_2, respectively, are known, Eqn. (3) was self-consistently solved over the range of ϕ - using C_p data from Figures 4. 2(d) and 4. 3, to determine the number of connected nanotubes: $N_{c,\,\phi 1}$ and $N_{c,\,\phi 2}$ at a given ϕ_1 and ϕ_2, respectively. The results of the above computational procedure are plotted in Figure 4. 4 and indicate an upward and a downward percolation like transition in the N_c and N_i, respectively. Such a plot seems to be in accord with the intuition of increasing cluster formation with enhanced nanotube filler concentration. We then think that the variation of the C_p with ϕ could indeed arise from the reorganization of the nanotubes, as depicted schematically in the insets to Figure 4. 4. The increasing degree of crystallinity up to ϕ_c, facilitated through nanotube connectivity, may correspond to an enhanced ordering in the polymer composite with a concomitant decrease in the composite entropy and the related C_p. In the sub-percolation threshold regime (with $\phi < \phi_c$) the nanostructures are relatively isolated, and evolve to an ordered polymer matrix spanning network at $\phi \sim \phi_c$. However, further increase of the nanotube content (at $\phi > \phi_c$) leads to uneven clustering and disorder, even as N_c was increased, implying an increased C_p. The reduction in the specific heat capacity of nanotube/polymer composites precisely near the electrical and thermal conductivity percolation threshold is remarkable in terms of thermal property modulation. It would be of much interest to explore the universal

validity of the observed phenomena related to the extent to which the C_p could be diminished as a function of the nanostructure aspect ratio as well as due to the influence of polymer matrix characteristics.

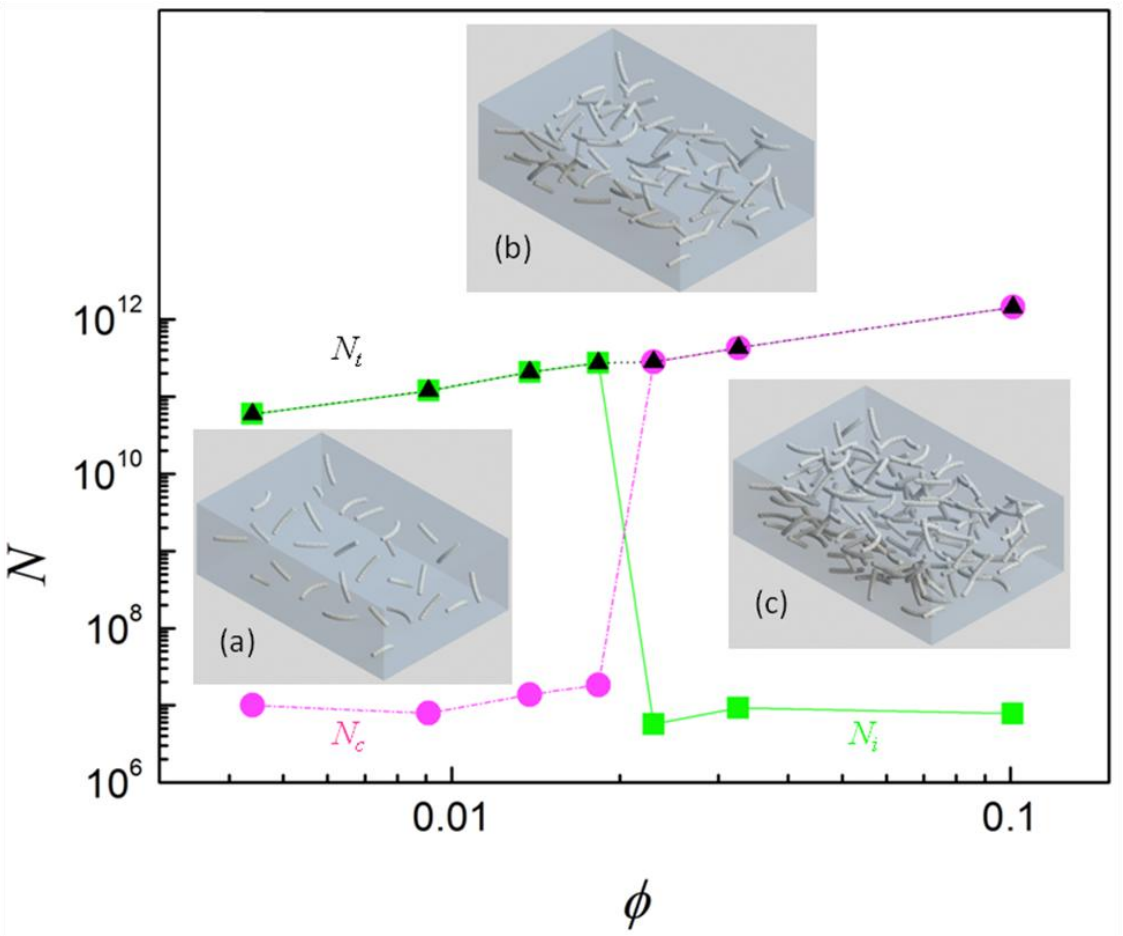

Figure 4. 4 The computed variation (from Eqn. 3) of the total number of CNTs (*Nt*) partitioned into isolated (*Ni*) or connected (*Nc*) constituents, *i.e.*, *Nt = Ni + Nc*. The *insets* (a), (b), and (c) indicate plausible arrangement of the nanostructures in the polymer matrix at $\phi < \phi_c$, $\phi = \phi_c$, and at $\phi < \phi_c$, respectively. The increase in nanotube ordering with φ corresponds to an increase in the *Nc* and a decreased *Cp*. Further increase of ϕ beyond ϕ_c induces clustering of the *Nc* and an increase of the *Cp*.

4. 4 Conclusions

In summary, we have reported a characteristic dip in the specific heat capacity of nanotube-polymer composites near the electrical and thermal conductivity percolation threshold. Such variation has been ascribed to the change in the ordering of the nanotubes from connected entities enhancing the crystallinity to cluster formation, below and above the percolation threshold, respectively.

4. 5 Acknowledgements

Chapter 4, in full, is a reprint of the material as it is under preparation for publication: Kim, B.-W., Park, S.-H., & P. R. Bandaru, Anomalous decrease of the specific heat capacity at the electrical and thermal conductivity percolation threshold in nanocomposites. *submitted* The dissertation author was the primary investigator and author of this paper.

4. 6 Supplementary information

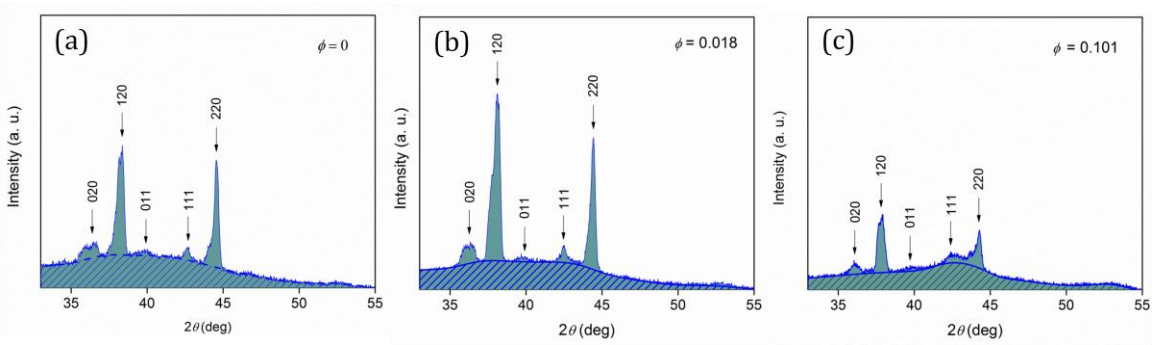

Figure 4. 5 XRD pattern at different CNT fractions: (a) $\phi = 0$, (b) $\phi = 0.018$, and (c) $\phi = 0.101$

Chapter 5: Summary of dissertation

The dissertation presented here investigated the electrical and thermal properties of CNT-polymer composites. Synthesizing such composite materials was successfully accomplished to uniformly disperse functionalized CNT fillers to be chemically linked with epoxide group of the polymer using a blend of solution and ultrasonication processing. Dependence of aspect ratio fillers on percolation threshold was experimentally observed and theoretically verified by the excluded volume method: thin and long CNTs are easy to make percolating networks, enhancing electrical and thermal conductivity within insulating matrix.

A consistent resistor model was constructed to understand thermal conduction within such nanostructure with analogy to the electrical conduction. Due to high electrical conductivity contrast between CNT and polymer (~15 orders of magnitude), electrical conducting along CNT networks dominates at or beyond percolation threshold. However, ~3 orders of magnitude difference of thermal conductivity between them allows non-negligible thermal conduction through the polymer. In addition, the effects of CNT orientation were studied: given volume fraction of CNTs aligned CNTs enhanced electrical/thermal conduction.

In the study of heat capacity, we have seen that the specific heat capacity of the composite materials reduced near the threshold. As the experimental result was initially unexpected and seminal, careful calibration and validation were conducted with two independent measurement manners, as well as degree of crystallinity supported the result.

We explained our experimental observation on the basis of Boltzmann entropy: forming CNT networks decreases degree of disorder, consequently heat capacity.

We expect our work to generate wide interest in the scientific community due to the tunability of thermal properties. We think that our demonstrations will have a major impact through providing insight into the inter-relationship of percolation and ordering and generate deep inquiry in exploring the universal validity of the observed phenomena.

REFERENCES

1. Cahill, D. G. & Pohl, R. O. Thermal conductivity of amorphous solids. *Phys. Rev. B* **35**, 4067 (1987)

2. Cahill, D. G. Thermal conductivity measurement from 30 to 750K: the 3ω method. *Rev. Sci. Instrum*. **61**, 802 (1990).

3. Chung, D. D. L. Electromagnetic interference shielding effectiveness of carbon materials. *Carbon* **39,** 279-285 (2001).

4. Al-Saleh, M. & Sundararaj, U. Electromagnetic interference (EMI) shielding effectiveness of PP/PS polymer blends containing high structure carbon black. *Macromol. Mater. Eng.* **293,** 621-630 (2008).

5. Park, S.-H., Thielemann, P., Asbeck, P. & Bandaru, P. R. Enhanced electromagnetic interfrence shielding through the use of functionalized carbon nanotube-reactive polymer composites. *IEEE Trans. Nanotechnol.* **9**, 464-469 (2009).

6. Rashid, E. S. A., Ariffin, K., Akil, H. M. & Kooi, C. C. Mechanical and Thermal Properties of Polymer Composites for Electronic Packaging Application. *J. Reinf. Plast. Comp.* **27**, 1573-1584 (2008).

7. Liu, Z., Bai, G., Huang, y., Li, F., Ma, Y., Guo, T., He, X., Lin, X., Gao, H., & Chen, Y. Microwave Absorption of Single-Walled Carbon Nanotubes/Soluble Cross-Linked Polyurethane Composites. *J. Phys. Chem. C* **111**, 13696-13700 (2007).

8. Lin, Y., Meziani, M. J., & Sun, Y.-P. Funtionalized carbon nanotubes for polymeric nanocomposites. *J. Mater. Chem*. **17,** 1143-1148 (2007).

9. Moniruzzaman, M. & Winey, K. I. Polymer nanocomposites containing carbon nanotubes. *Macromol*. **39,** 5194-5205 (2006).

10. Li, N., Huang, Y., Du, F., He, X., Lin, X., Gao, H., Ma, Y., Li, F., Chen, Y., & Eklund, P. C. Electromagnetic interference (EMI) shielding of single-walled nanotube epoxy composites. *Nanolett.* **6,** 1141-1145 (2006).

11. Saib A., Bednarz, L., Daussin, R., Bailly, C., Lou, X., Thomassin, J. M., Pagnoulle, C., Detrembleur, C., Jérôme, R., & Huynen, I. Carbon nanotube composites for broadband microwave absorbing materials. *IEEE Tran.s Microw. Theory Tech.* **54,** 2745-2754 (2006).

12. Ajayan, P. M., Schadler, L. S., Giannaris, C., & Rubio, A. Single-walled carbon nanotube-polymer composites: strength and weakness. *Adv. Mater*. **12,** 750-753 (2000).

13. Kirkpatrick, S. Percolation and conduction. *Rev. Mod. Phys.* **45,** 574-588 (1973).

14. Nicholas, J. A., Saito, H., Deck, C., & Bandaru, P. R. Artificial introduction of defects into vertically aligned multiwalled carbon nanotube ensembles: Application to electrochemical sensors. *J. Appl. Phys.* **102,** 064306 (2007).

15. Pfeifer, S., Park, S. H. & Bandaru, P. R. A methodology for quantitatively characterizing the dispersion of nanostructures in polymers and composite. *J. Appl. Phys*. **108,** 024305 (2010).

16. Berber, S., Kwon, Y.-K., & Tomanek, D. Unusually high thermal conductivity of carbon nanotubes. *Phys. Rev. Lett*. **84**, 4613 (2000).

17. Bandaru, P. R. Electrical properties and applications of carbon nanotube structures. *J. Nanosci. Nanotechnol*. **7**, 1239 (2007).

18. Ci, L., Suhr, J., Pushparaj, V., Zhang, X., & Ajayan, P. M. Continuous carbon nanotube reinforced composites, *Nanolett* **8**, 2762 (2008).

19. Bigg, D. M., & Stutz, D. E. Plastic composites for electromagnetic interference shielding application. *Polym. Comp.* **4**, 40 (1983).

20. Hughes, M. in *Dekker Encyclopedia of Nanoscience and Nanotechnology* (Taylor & Francis, London, 2004), p. 447.

21. Pfeifer, S. & Bandaru, P. R. *Polyme*r (in press) (2011).

22. Park, S.-H., Thielemann, P., Asbeck, P. & Bandaru, P. R. Enhanced dielectric constants and shielding effectiveness of uniformly dispersed functionalized carbon nanotube composites**.** *Appl. Phys. Lett*. **94**, 243111 (2009).

23. Balberg, I., Anderson, C. H., Alexander, S., & Wagner, N. Excluded volume and its relation to the onset of percolation. *Phys. Rev. B* **30**, 3933 (1984).

24. Celzard, A. McRae, E., Deleuze, C., Dufort, M., Furdin, G. & Mareche, J. F. Critical concentration in percolating systems containing a high-aspect ratio filler. *Phys. Rev. B* **53**, 6209 (1996).

25. Stauffer, D. & Aharony, A. *Introduction to Percolation Theory* (CRC Press, Boca Raton, FL, 1994).

26. White, S. L., DiDonna, B. A., Mu, M., Lubensky, T. C. & Winey, K. I. Simulations and electrical conductivity of percolated networks of finite rods with various degrees of axial alignment. *Phys. Rev. B* **79**, 024301 (2009).

27. Du, F., Fischer, J. E., & Winey, K. I. Effect of nanotube alignment on percolation conductivity in carbon nanotube/polymer composites. *Phys. Rev. B* **72**, 121404(R) (2005).

28. Carslaw, H. S. & Jaeger, J. C. *Conduction of Heat in Solids* (Oxford University Press, New York, 1986).

29. Borca-Tasciuc, T., Kumar, A. R. & Chen, G. Data reduction in 3w method for thin-film thermal conductivity measurement. *Rev. Sci. Instrum.* **72**, 2139 (2001).

30. Foygel, M., Morris, R. D., Anez, D., French, S. & Sobolev, V. L. Theoretical and computational studies of carbon nanotube composites and suspensions: Electrical and thermal conductivity. *Phys. Rev. B* **71**, 104201 (2005).

31. Shklovskii, B. I. & Efros, A. L. *Electronic Properties of Doped Semiconductors* (Springer-Verlag, New York, NY, 1984).

32. Straley, J. P. Critical exponents for the conductivity of random resistor lattices. *Phys. Rev. B* **15**, 5733 (1977).

33. Huxtable, S. T., Cahill, D. G., Shenogin, S., Xue, L., Ozsik, R., Barone, P., Usrey, M., Strano, M. S., Siddons, G., Shim, M. & Keblinski, P. Interfacial heat flow in carbon nanotube suspension, *Nat Mater* **2**, 731 (2003).

34. Shenogina, N., Shenogin, S., Xue, L. & Keblinski, P. On the lack of thermal percolation in carbon nanotube composites. *Appl. Phys. Lett*. **87** 133106 (2005).

35. Biercuk, M. J., Llaguno, M. C., Radosavljevic, M., Hyun, J. K., Johnson, A. T. & Fischer, J. E. Carbon nanotube composites for thermal management. *Appl. Phys. Lett*. **80**, 2767 (2002).

36. Bonnet, P., Sireude, D., Garnier, B. & Chauvet, O. Thermal properties and percolation in carbon nanotube-polymer composites. *Appl. Phys. Lett*. **91**, 201910 (2007).

37. Landauer, R. Electrical conductivity in inhomogeneous media. *AIP Conf. Proc*. **40**, 2 (1978).

38. Thomas, S., Joseph, K., Malhotra, S. K., Goda, K. & Sreekala, M. S. *Polymer Composites*. (Wiley-VCH, 2013).

39. De Volder, M. F. L., Tawfick, S. H., Baughman, R. H. & Hart, A. J. Carbon nanotubes: present and future commercial applications. *Science* **339,** 535–9 (2013).

40. Baughman, R. H., Zakhidov, A. A. & de Heer, W. A. Carbon Nanotubes - the Route Toward Applications. *Science* **29,** 787–792 (2002).

41. Ambrosetti, G., Grimaldi, C., Balberg, I., Maeder, T., Danani, A. & Ryser, P. Solution of the tunneling-percolation problem in the nanocomposite regime. *Phys. Rev. B* **81,** 155434 (2010).

42. Coleman, J. N., Khan, U., Blau, W. J. & Gun'ko, Y. K. Small but Strong: A review of the mechanical properties of carbon nanotube-polymer composites. *Carbon N. Y.* **44,** 1624–1652 (2006).

43. Pfeifer, S., Park, S. H. & Bandaru, P. R. Analysis of electrical percolation thresholds in carbon nanotube networks using the Weibull probability distribution. *J. Appl. Phys*. **108**, 24305 (2010)

44. Bauhofer, W. & Kovacs, J. Z. A review and analysis of electrical percolation in carbon nanotube polymer composites. *Compos. Sci. Technol.* **69,** 1486–1498 (2009).

45. Kim, B.-W., Park, S.-H., Kapadia, R. S. & Bandaru, P. R. Evidence of percolation related power law behavior in the thermal conductivity of nanotube/polymer composites. *Appl. Phys. Lett.* **102,** 243105 (2013).

46. Pfeifer, S. & Bandaru, P. R. A Methodology for Quantitatively Characterizing the Dispersion of Nanostructures in Polymers and Composites. *Mater. Res. Lett.* 1–10 (2014). doi:10.1080/21663831.2014.886629

47. Vionnet-Menot, S., Grimaldi, C., Maeder, T., Strassler, S. & Ryser, P. Tunneling percolation origin of nonuniversality: Theory and experiments. *Phys. Rev. B* **71,** 64201 (2005).

48. Schutz, R. J. Thermal relaxation calorimetry below 1 K. *Rev. Sci. Instrum.* **45,** 548 (1974).

49. Lide, D. R. *CRC Handbook Chemistry and Physics*. (2004).

50. Koerner, H., Price, G., Pearce, N. A., Alexander, M. & Vaia, R. A. Remotely actuated polymer nanocomposites--stress-recovery of carbon-nanotube-filled thermoplastic elastomers. *Nat. Mater.* **3,** 115–20 (2004).

51. Wunderlich, B. Motion in Polyethylene. I. Temperature and Crystallinity Dependence of the Specific Heat. *J. Chem. Phys.* **37,** 1203 (1962).

52. D'Angelo, G., Tripodo, G., Carini, G., Bartolotta, A., Di Marco, G. & Salvato, G. Low-temperature excess specific heat and fragility in polymers: Crystallinity dependence. *J. Chem. Phys.* **109,** 7625 (1998).

53. Walter, E. R. & Reding, F. P. Variations in unit cell dimensions in polyethylene. *J. Polym. Sci.* **21,** 561–562 (1956).

54. Balberg, I., Azulay, D., Toker, D. & Millo, O. Percolation and Tunneling in Composite Materials. *Int. J. Mod. Phys. B* **18,** 2091–2121 (2004).

55. Tsu, R. Critical volume fraction of crystallinity for conductivity percolation in phosphorus-doped Si:F:H alloys. *Appl. Phys. Lett.* **40,** 534 (1982).

56. Scher, H. Critical Density in Percolation Processes. *J. Chem. Phys.* **53,** 3759 (1970).

57. Gonzalez-Hernandez, J., Martin, D., Chao, S. S. & Tsu, R. Structural dependence of percolation in germanium films. *Appl. Phys. Lett.* **44,** 672 (1984).

58. Callen, H. B. *Thermodynamics*. (John Wiley Inc., 1960).